2 mip

NASA TECHNICAL NOTE

NASA TN D-7582

NASA TN D-7582

A SYSTEM FOR SPACECRAFT ATTITUDE CONTROL AND ENERGY STORAGE

by John D. Shaughnessy

Langley Research Center

Hampton, Va. 23665

NATIONAL AERONAUTICS AND SPACE ADMINISTRATION • WASHINGTON, D. C. • AUGUST 1974

1. Report No.	2. Government Accession No.	3. Recipient's Catalog No.
NASA TN D-7582		

4. Title and Subtitle	5. Report Date
A SYSTEM FOR SPACECRAFT ATTITUDE CONTROL AND ENERGY STORAGE	August 1974
	6. Performing Organization Code

7. Author(s)	8. Performing Organization Report No.
John D. Shaughnessy	L-9271
	10. Work Unit No.
9. Performing Organization Name and Address	502-23-44-02
NASA Langley Research Center Hampton, Va. 23665	11. Contract or Grant No.
	13. Type of Report and Period Covered
12. Sponsoring Agency Name and Address	Technical Note
National Aeronautics and Space Administration Washington, D.C. 20546	14. Sponsoring Agency Code

15. Supplementary Notes

The information in this paper is largely based on a thesis submitted in partial fulfillment of the requirements for the degree of Doctor of Philosophy in Aerospace Engineering, Virginia Polytechnic Institute and State University, Blacksburg, Virginia, November 1973.

16. Abstract

A conceptual design for a double-gimbal reaction-wheel—energy-wheel device which has three-axis attitude control and electrical energy storage capability is given. A matnematical model for the three-axis gyroscope (TAG) is developed, and a system of multiple units is proposed for attitude control and energy storage for a class of spacecraft. Control laws are derived to provide the required attitude-control torques and energy transfer while minimizing functions of TAG gimbal angles, gimbal rates, reaction-wheel speeds, and energy-wheel speed differences. A control law is also presented for a magnetic torquer desaturation system. To evaluate the concept, a computer simulation of a three-TAG system for an orbiting telescope is used. The results of the study indicate that all control and power requirements can be satisfied by using the TAG concept.

17. Key Words (Suggested by Author(s))	18. Distribution Statement
Control moment gyro Energy storage Three-axis attitude control Hybrid real-time simulation Reaction wheels	Unclassified – Unlimited STAR Category 31

19. Security Classif. (of this report)	20. Security Classif. (of this page)	21. No. of Pages	22. Price*
Unclassified	Unclassified	86	$4.00

*For sale by the National Technical Information Service, Springfield, Virginia 22151

CONTENTS

A SYSTEM FOR SPACECRAFT ATTITUDE CONTROL AND ENERGY STORAGE*

By John D. Shaughnessy
Langley Research Center

SUMMARY

A conceptual design for a double-gimbal reaction-wheel—energy-wheel device which has three-axis attitude control and electrical energy storage capability is given. A mathematical model for the three-axis gyroscope (TAG) is developed, and a system of multiple TAG units with a digital flight computer is proposed for attitude control and energy storage for spacecraft application. Algorithms that determine torques required for spacecraft fine pointing, coarse pointing, and reorientation are formulated. Control laws are derived to provide the required spacecraft attitude control while minimizing functions of TAG gimbal angles, gimbal rates, reaction-wheel speeds, and energy-wheel speed differences. A magnetic torquer is proposed for system desaturation, and a control law that minimizes magnetic power consumption, while providing management of angular momentum each orbit, is derived.

To evaluate the concept, a three-TAG system is sized for the A303B advanced solar observatory mission which is a proposed shuttle-launched research and applications module (RAM); and a computerized research simulation of the TAG system and spacecraft dynamics is developed and used. Various modes of operation, including spacecraft fine pointing in the presence of time-varying gravity-gradient disturbance torques, are considered. Time-history plots of critical variables are presented and discussed for the cases studied.

The results of the study indicate the following. Three-axis attitude control and energy storage using the TAG concept is feasible. In the derivation of the gimbal rate control law, minimizing the sum of squares of gimbal angles plus their rates minimizes the power required and causes the gimbals to favor their reference orientation continuously. The reaction wheels can be continuously desaturated without causing any net torque on the spacecraft by combined reaction-wheel speed feedback and controlled precession of the gimbals. Using the TAG units for energy storage causes the angular momentum

*The information in this paper is largely based on a thesis submitted in partial fulfillment of the requirements for the degree of Doctor of Philosophy in Aerospace Engineering, Virginia Polytechnic Institute and State University, Blacksburg, Virginia, November 1973.

level to be significantly higher than necessary for control only. For the example mission studied, the pointing errors caused by gravity-gradient torques are controlled to less than 0.017 arc second.

INTRODUCTION

Earth orbital missions including Skylab and the proposed space-shuttle-launched research applications modules (RAM's) studied under contract NAS 8-27539 (designated the RAM study herein), as well as other missions, require attitude-control subsystems for spacecraft fine pointing and reorientation. These missions also require subsystems to generate continuous electrical power for spacecraft and payload. Various arrangements of reaction jets, momentum exchange devices, and magnetic torquers are used for attitude control and stabilization, and solar cell arrays with batteries and fuel cells are used for electrical-power generation and storage. Each of these systems has limiting characteristics which make it undesirable for meeting all mission requirements. In the area of attitude control, reaction wheels (refs. 1 to 3), both fixed and gimbaled, can produce very precise fine pointing control, but are not efficient when used to counteract long-term torques such as those caused by gravity gradients. Control-moment gyroscopes (CMG's) (refs. 4 to 7) of the double gimbal type can efficiently produce large transfers of momentum but are not suitable for producing the precise high-frequency torques necessary to meet high pointing stability requirements. Reaction jet control systems are not efficient as primary attitude controllers for long duration missions because of the high weight penalty associated with the onboard fuel requirements. Magnetic torquers (conceptually studied by W. Levidow and discussed in ref. 8) are not viable for primary control tasks because control torques cannot be generated along the lines of the Earth's magnetic flux which run approximately north and south. Reaction jets and magnetic torquers are, however, useful in the desaturation of momentum storage systems.

To date, the most used electrical energy storage device is the nickel cadmium (NiCd) battery. Even though these batteries are used extensively, they have several fundamental problems that must be considered in the design of a long-life energy-storage system. Research indicates that battery lifetime and performance are seriously affected by such factors as depth of discharge, number of charge-discharge cycles, temperature variation, and charge-discharge rates. In near-Earth orbits these factors tend to reach their maximum values and hence have the most effect. Fuel cells are primarily used only for short-term missions because of the fuel weight penalty in long missions.

It has been suggested by R. Gorman that spacecraft solar array/battery systems be replaced by solar array/flywheel-motor-generator systems. Furthermore, mounting the flywheels in gimbals would result in a system capable of performing the dual function of attitude control and energy storage. Studies by Lawson and Rabenhorst in references 9

and 10 have indicated that new materials and design techniques will permit the development of high-speed flywheels that have high-energy densities. In comparison with the state-of-the-art batteries, the flywheels offer potential weight savings in addition to higher efficiency and reliability. Also, the fundamental problems associated with batteries mentioned earlier are minimal or nonexistent with flywheel-motor generators.

The Langley Research Center has supported a 1-year study (refs. 11 and 12) to determine the feasibility of a dual-function flywheel system. This effort is referred to as the IPACS study throughout the remainder of this analysis. The IPACS study has shown that for near-Earth orbit missions of long duration with medium to high pointing accuracy requirements, and medium power levels, the dual function concept is feasible.

Anderson and Keckler in reference 13 have considered single-rotor and double-rotor IPACS units for attitude control and energy storage. Their simulations have not indicated any major problems associated with the dual-function concept as far as the capability of the units to overcome the independent requirements that a spacecraft's subsystem's power demands would place on the unit's flywheels for the configuration/mission simulated. There are, however, minor interactions between momentum and energy storage that result from hardware requirements. These interactions include a decrease in low-level torque capability caused by increased gimbal friction resulting from larger sliprings to carry power to and from the spin assembly, and increased control computer requirements to handle complex control algorithms.

Because each system concept is limited, combinations of systems are used in order to meet mission requirements. For example, in Skylab, CMG's are used for coarse pointing and reorientation, and direct-drive torquers control the telescope array with respect to the main vehicle for fine pointing. In the shuttle-launched RAM spacecraft, CMG's are proposed for coarse pointing and reorientation; reaction wheels, for fine pointing. In both of these missions NiCd batteries are used for energy storage.

This analysis presents a conceptual design for a double-gimbal reaction-wheel—energy-wheel device which is capable of producing fine pointing torques, coarse pointing and reorientation torques, and electrical energy storage. A redundant system of two or more of these units, each referred to as a three-axis gyroscope (TAG), is considered in general terms for a class of spacecraft, and the necessary control algorithms are derived. These control algorithms are designed to produce the required spacecraft control torques and the energy transfer while minimizing functions of TAG gimbal angles, gimbal rates, reaction-wheel speeds, and energy-wheel speed differences. A control law is also derived for a magnetic torquer desaturation system.

To evaluate the concept, a three-TAG system is applied to one of the proposed free-flying shuttle/RAM payloads. The units are sized, and control gains are determined to meet the mission attitude control and power requirements. A hybrid computer simulation

of the spacecraft/TAG system is developed and used for real-time evaluation and verification of the TAG system performance and capability.

SYMBOLS

A bar under a symbol indicates a column matrix or vector quantity. Dots over a symbol denote derivatives with respect to time. A vector symbol enclosed in brackets $[\ ]$ indicates a special skew symmetric matrix. For example, let

$$\underline{r} = \begin{bmatrix} r_x & r_y & r_z \end{bmatrix}^T$$

Then,

$$[\underline{r}] \triangleq \begin{bmatrix} 0 & -r_z & r_y \\ r_z & 0 & -r_x \\ -r_y & r_x & 0 \end{bmatrix}$$

A	TAG unit reaction torque coefficient matrix defined by equation (4)
$\underline{B}$	Earth's magnetic field flux vector
C	gimbal rate-control-law matrix, $Q^{-1}\Gamma^T(\Gamma Q^{-1}\Gamma^T)^{-1}$
D	determinant of $\tilde{R}\tilde{R}^T$
E_T	TAG system kinetic energy defined by equation (30)
F_A	outer gimbal angle gain in equation (18)
F_B	inner gimbal angle gain in equation (19)
$\underline{f}(\gamma)$	gimbal angle functions defined by equations (18) and (19)
G	reaction-wheel control law matrix, $\tilde{R}^T(\tilde{R}\tilde{R}^T)^{-1}$
H	energy-wheel average spin momentum magnitude, $\frac{1}{n}\sum_{i=1}^{n} I_{HA}\omega_{Hi}$

$\tilde{H}$	matrix of spin momentum magnitudes, $\text{diag}\left(H_1 \ldots H_n \quad H_1 \ldots H_n\right)$
$\underline{H}$	matrix of spin momentum magnitudes, $\left[H_1 \ldots H_n\right]^T$
$\underline{H}_b$	bias momentum to be dumped
$\underline{H}_I$	inner gimbal angular momentum
$\underline{H}_O$	outer gimbal angular momentum
$\underline{H}_S$	spacecraft angular momentum excluding the TAG units
$\underline{H}_T$	TAG unit total angular momentum vector given by equation (2)
$\underline{H}_W$	angular momentum of reaction wheel plus angular momentum of energy wheel
I	identity matrix
I_H	energy-wheel inertia matrix, $\text{diag}\left(I_{HT} \quad I_{HA} \quad I_{HT}\right)$
I_{HA}, I_{HT}	energy-wheel axial and transverse moments of inertia
I_I	inner gimbal inertia matrix
I_L	reaction-wheel inertia matrix, $\text{diag}\left(I_{LT} \quad I_{LA} \quad I_{LT}\right)$
I_{LA}, I_{LT}	reaction-wheel axial and transverse moments of inertia
I_O	outer gimbal inertia matrix
I_S	spacecraft inertia matrix
I_T	axisymmetric spacecraft transverse moment of inertia
I_x, I_y, I_z	spacecraft moments of inertia about principal axes
i, j	integers
J_M	magnetic torquer cost function

J_p gimbal rate control law cost function

J_p^* constrained gimbal rate control law cost function

J_R reaction wheel control law cost function

J_R^* constrained reaction wheel control law cost function

K_{AC} coarse pointing attitude gain matrix, diag $\begin{pmatrix} K_{ACx} & K_{ACy} & K_{ACz} \end{pmatrix}$

K_{AF} fine pointing attitude gain matrix, diag $\begin{pmatrix} K_{AFy} & K_{AFz} \end{pmatrix}$

KF gimbal angle function gain, $KF = F_A$ for $i = 1, \ldots, n$ and $KF = F_B$ for $i = n + 1, \ldots, 2n$

K_R reaction-wheel desaturation gain

K_{RC} coarse pointing rate gain matrix, diag $\begin{pmatrix} K_{RCx} & K_{RCy} & K_{RCz} \end{pmatrix}$

K_{RF} fine pointing rate gain matrix, diag $\begin{pmatrix} K_{RFx} & K_{RFy} & K_{RFz} \end{pmatrix}$

K_{RM} reorientation rate gain matrix, diag $\begin{pmatrix} K_{RMx} & K_{RMy} & K_{RMz} \end{pmatrix}$

k energy equalization time constant

$\underline{M}$ magnetic moment, $\begin{bmatrix} M_x & M_y & M_z \end{bmatrix}^T$

m integer, $m = 1$ for maneuvers and $m = 0$ for pointing

n number of TAG units in system

P_C charging power available in sunlight

P_D discharge power with simultaneous experiment operation

P_{DP} peak discharge power increment

P_T mechanical power required to torque energy wheels

p,q,r inertially referenced body rates

Q diagonal gimbal rate weighting matrix, $\text{diag}(q_1 \cdots q_n)$

R spin-rate transformation matrix defined by equation (12)

$\tilde{R}$ R matrix with first row deleted given by equation (23)

$RR_{11}, RR_{12}, RR_{22}$ factors in G matrix

$\hat{r}$ unit vector

$s(\,), c(\,)$ sin( ) and cos( ), respectively

$\underline{T}_A$ TAG wheel acceleration torque given by equation (15)

$\underline{T}_B$ torque due to attached magnet

$\underline{T}_{CD}$ desired spacecraft coarse pointing control torque defined by equation (5)

$\underline{T}_D$ gravity-gradient torque vector

$\underline{T}_{D,max}$ maximum gravity-gradient torque

$\underline{T}_{FD}$ desired spacecraft two-axis fine pointing control torque defined by equation (6)

$\underline{T}_G$ desired TAG precession torque defined by equation (16)

$\underline{T}_H$ matrix of energy-wheel control torques, $\left[T_{H1} \cdots T_{Hn}\right]^T$

$\underline{T}_{HC}$ matrix of energy-wheel torque commands defined by equation (32)

$T_{I/B}$ inertial axes to spacecraft body axes transformation matrix

$T_{I/S}$ inner gimbal to spacecraft axes transformation matrix

$\underline{T}_L$ matrix of reaction-wheel control torques, $\left[T_{L1} \cdots T_{Ln}\right]^T$

$\underline{T}_{LD}$ desired value of $\underline{T}_L$

$\underline{T}_{LS}$ reaction-wheel torque in spacecraft coordinates, $-R\underline{T}_L$

$\underline{T}_{MD}$ desired spacecraft maneuver control torque defined by equation (7)

T_O orbital period

$T_{O/S}$ outer gimbal to spacecraft axes transformation matrix

$\underline{T}_P$ TAG system precession torque given by equation (14)

$\underline{T}_R$ total wheel acceleration torque acting on spacecraft, $-R\left(\underline{T}_L + \underline{T}_H\right)$

$\underline{T}_T$ TAG system output torque given by equation (8)

$\underline{T}_U$ TAG unit output torque given by equation (1)

t time

X_I, Y_I, Z_I inertial axes

X_O, Y_O, Z_O orbit reference axes

x_I, y_I, z_I inner gimbal axes

x_O, y_O, z_O outer gimbal axes

x_S, y_S, z_S spacecraft axes (used without S as subscripts)

α, β outer and inner gimbal angles

α_i, β_i ith unit outer and inner gimbal angles

α_{iO}, β_{iO} ith unit reference gimbal angles

Γ TAG system matrix given by equation (11)

$\underline{\gamma}$ TAG system gimbal angle matrix, $\left[\alpha_1 \cdots \alpha_n \quad \beta_1 \cdots \beta_n\right]^T$

$\underline{\dot{\gamma}}_D$ desired TAG system gimbal rate matrix

ϵ_i ith energy-wheel energy error defined in equation (29)

θ spacecraft pitch angle defined in figure 10

$\underline{\theta}$ spacecraft angular position matrix, $\lfloor \phi \quad \theta \quad \psi \rfloor^T$

$\underline{\theta}_C$ measured coarse pointing attitude error $\lfloor \phi_C \quad \theta_C \quad \psi_C \rfloor^T$ where C denotes coarse

$\underline{\theta}_F$ measured two-axis fine pointing attitude error $\lfloor \theta_F \quad \psi_F \rfloor^T$ where F denotes fine

$\underline{\theta}_0$ initial angular position vector $\lfloor \phi_0 \quad \theta_0 \quad \psi_0 \rfloor^T$ where 0 denotes time zero

$\underline{\lambda}$ vector of Lagrange multipliers, $\lfloor \lambda_1 \quad \lambda_2 \quad \lambda_3 \rfloor^T$

ρ controlled spacecraft theoretical damping ratio

τ dummy variable of integration

ϕ spacecraft roll angle defined in figure 10

ψ spacecraft yaw angle defined in figure 10

$\underline{\Omega}$ spacecraft inertially referenced body rates, $\lfloor p \quad q \quad r \rfloor^T$

$\underline{\Omega}_C$ measured coarse pointing angular rate error $\lfloor p_C \quad q_C \quad r_C \rfloor^T$ where C denotes coarse

$\underline{\Omega}_F$ measured two-axis fine pointing angular rate error $\lfloor q_F \quad r_F \rfloor^T$ where F denotes fine

$\underline{\Omega}_M$ measured reorientation rate vector $\lfloor p_M \quad q_M \quad r_M \rfloor^T$ where M denotes maneuver

$\underline{\Omega}_{MD}$ desired reorientation rate vector $\lfloor p_{MD} \quad q_{MD} \quad r_{MD} \rfloor^T$ where D denotes desired value

$\underline{\omega}_H$ matrix of energy-wheel spin rates, $\lfloor \omega_{H1} \cdots \omega_{Hn} \rfloor^T$

$\underline{\omega}_H^I$ energy-wheel angular velocity with respect to inner gimbal

$\underline{\omega}_I$ inner gimbal angular velocity with respect to spacecraft

$\underline{\omega}_L$ matrix of reaction-wheel spin rates, $\left[\omega_{L1} \cdots \omega_{Ln}\right]^T$

$\underline{\omega}_L^I$ reaction-wheel angular velocity with respect to inner gimbal

ω_O orbital frequency

$\underline{\omega}_O$ outer gimbal angular velocity with respect to spacecraft

Superscripts:

I inner gimbal coordinates

O outer gimbal coordinates

R inertial coordinates

S spacecraft coordinates

Mathematical:

$(\,)^{-1}$ inverse of ( )

$(\,)^T$ transpose of ( )

$\approx$ approximately equal

$[\ ]$ rectangular matrix or special skew symmetric matrix

$\langle\ \rangle$ column matrix

$[\ ]$ row matrix

$>>$ much greater than

diag ( ) ( ) is diagonal

$\triangleq$ definition

$\text{sgn}(\,)$	sign of ( )
$\frac{\partial x}{\partial y}$	partial derivative of x with respect to y
$\frac{dx}{dt}$	total derivative of x with respect to t
$\int (\,)\, d\tau$	integral of ( ) with respect to τ
$\sum_{i=1}^{n} (\,)$	summation of ( ) from $i = 1$ to $i = n$

Abbreviations:

ADC	analog to digital converter
CMG	control moment gyroscope
DAM	digital to analog multiplier
DCA	digitally controlled attenuator
IPACS	integrated power and attitude control system
RAM	research applications module
TAG	three-axis gyroscope

CONCEPT DEFINITION AND ANALYSIS

TAG Unit Concept

A general description of the TAG unit is followed by a development of the TAG mathematical model and torque equation. The principle of operation is discussed, and the TAG system concept is introduced.

Unit description.- The TAG unit shown in figure 1 is basically a double-gimbal gyroscope with an inner gimbal assembly comprised of a high-speed energy wheel spinning coaxially inside of a low-speed reaction wheel which also could serve as a safety shield for the energy wheel. Tachometers are used to provide wheel-speed information. The inner gimbal assembly is suspended in an outer gimbal with the inner gimbal axis normal to the wheels' spin axes. The inner gimbal is servo driven with respect to the

outer gimbal with tachometers and resolvers used to measure inner gimbal rates and angles with respect to the outer gimbal. The outer gimbal is suspended in a mounting structure with the outer gimbal axis normal to the inner gimbal axis. The outer gimbal is servo driven with respect to the mounting frame, and tachometers and resolvers are used to measure outer gimbal rates and positions. The mounting frame is used to attach the TAG unit to the spacecraft.

TAG mathematical model.- It is assumed that the TAG unit may be represented mathematically by a combination of four rigid elements as shown in figure 1. These elements are the two axisymmetric wheels, the inner gimbal, and the outer gimbal. A moving spacecraft axis system is used as reference for the TAG components as shown in figures 2 and 3. It is also assumed that, for each element, geometric axes are principal axes, and the wheels' spin axis is coincident with the inner gimbal y_I-axis as shown in figure 3.

The output torque equation for the TAG unit, derived in appendix A, is

$$\underline{T}_U^S = -\dot{\underline{H}}_T^S - \left[\underline{\Omega}\right]\underline{H}_T^S \tag{1}$$

where the TAG unit total angular momentum is given by

$$\begin{aligned}\underline{H}_T^S = {} & T_{O/S}{}^I{}_O\underline{\omega}_O^O + T_{O/S}{}^I{}_O T_{O/S}^T\underline{\Omega} + T_{I/S}{}^I{}_I\underline{\omega}_I^I + T_{I/S}{}^I{}_I T_{I/S}^T\underline{\Omega} \\ & + T_{I/S}{}^I{}_L\left(\underline{\omega}_L^I + \underline{\omega}_I^I + T_{I/S}^T\underline{\Omega}\right) + T_{I/S}{}^I{}_H\left(\underline{\omega}_H^I + \underline{\omega}_I^I + T_{I/S}^T\underline{\Omega}\right)\end{aligned} \tag{2}$$

For the case of interest the spacecraft angular rates are much smaller than the normal gimbal rates; the spin momentum of the energy wheel is orders of magnitude larger than that of the gimbals or reaction wheel; and the acceleration torque of either wheel is much larger than that of the gimbals. Thus, the torque equation may be approximated by

$$\underline{T}_U^S = HA\left[\dot{\alpha} \quad \dot{\beta} \quad \dot{H}/H\right]^T \tag{3}$$

where $\dot{\alpha}$ and $\dot{\beta}$ are the relative angular rates of the outer gimbal and inner gimbal, respectively, and $\dot{H}$ is the rate of change of the wheels' spin momentum magnitude H. The transformation matrix A is given by

$$A = \begin{bmatrix} 0 & c\beta & s\beta \\ c\beta s\alpha & s\beta c\alpha & -c\beta c\alpha \\ -c\beta c\alpha & s\beta s\alpha & -c\beta s\alpha \end{bmatrix} \tag{4}$$

Principle of operation.- If the TAG outer and inner gimbals are driven at rates $\dot{\alpha}$ and $\dot{\beta}$, respectively, and if the wheels are accelerated so that $\dot{H}$ is nonzero, then the TAG reaction torque exerted on the spacecraft will be the three-axis torque $\underline{T}_U^S$ given by equation (1) and approximated by equation (3). Equation (3) indicates that by actively controlling the gimbal rates $\dot{\alpha}$ and $\dot{\beta}$ and the total wheel acceleration $\dot{H}/H$, the components of the torque $\underline{T}_U^S$ can be controlled. If two or more units are used, then the torque due to reaction-wheel acceleration is used for fine pointing, and the torque due to the gimbal rates is used to counteract the gravity-gradient torque and produce a reorientation torque.

Electrical energy is stored in the TAG by accelerating the energy wheel to higher speeds. Energy is transferred back to the spacecraft by using a generator attached to the energy wheel. A net reaction torque on the spacecraft, during energy transfer, is avoided by the use of two or more TAG units and by "scissoring" the individual angular momentum vectors to cancel the effect of varying momentum magnitudes.

Since most spacecraft attitude control and energy storage systems are designed to be redundant, it is practical to consider a multiple TAG system where two or more units are used. Such a system would provide fine pointing control by accelerating the reaction wheels. Coarse pointing and reorientation control would be generated by driving the gimbals in a controlled manner. Energy storage would be accomplished by accelerating only the energy wheels while the individual momentum vectors would be scissored to maintain the desired angular momentum.

TAG System Concept

In this section the TAG system configuration is described, and a discussion of the system control law philosophies is given.

TAG system description.- The TAG system concept is shown pictorially in block diagram form in figure 4. The system consists of at least two TAG units together with spacecraft attitude sensor equipment, a digital flight computer, and a solar array.

The axis system for the TAG units is shown in figure 5 and is taken so that the outer gimbal axes are parallel to the spacecraft's pointed axis. This configuration tends to minimize inner gimbal motion since the gravity gradient torque is normal to the pointed axis; a roll symmetric spacecraft with its roll axis being the pointed axis is assumed.

The reference inner gimbal angles are taken as 0°. This assumption gives equal positive and negative inner gimbal travel before the critical $\pm 90^\circ$ limit is reached. Also, for two-axis fine pointing, assumed here, it is desired to maintain the reaction-wheel spin axes normal to the pointed axis so that electrical power is not wasted by generating unwanted reaction-wheel torques about the pointed axis.

For systems with three or more TAG units the reference outer gimbal angles are taken so that the sum of the momentum vectors is equal to zero. This arrangement implies 120° separation for a three TAG system, 90° separation for a four TAG system, and so forth. For a two TAG system, equal separation (180°) would result in loss of fine pointing reaction-wheel control about the axis normal to the colinear vectors. In that case, 90° separation is suggested. Zero total angular momentum is taken as reference since it gives the control system a spherical operating envelope. Also, prior to initiating large-angle reorientations, it is desired to have zero net angular momentum so that as the spacecraft reorientation rate develops, the net TAG system angular momentum will develop along the maneuver axis. This condition allows the gimbals to remain stationary with respect to the spacecraft once the rate is acquired and avoids undesirable momentum vector orientations and/or mechanical gimbal stop encounters during the maneuver.

Attitude control.- The attitude-control function operates as follows. (See fig. 4.) Attitude control commands are telemetered from the ground and/or generated onboard the spacecraft and are entered into the flight computer. Sensors, such as star trackers, Sun sensors, inertial measuring units, and experiment integral sensors are used to determine current attitude data. The attitude command signals are compared with the measured spacecraft attitude data and error signals are computed. These error signals are used to compute the desired nulling torques for maneuvering or pointing the spacecraft.

The three-axis spacecraft coarse pointing and reorientation control torques are generated by driving the TAG gimbals. A control law computes the command gimbal rates, in terms of the desired coarse pointing or reorientation torques and TAG gimbal angles and angular momentum, to correct spacecraft angle and angular rate errors and to minimize functions of TAG gimbal angles and rates continuously.

Two-axis spacecraft fine pointing torques are generated by the reaction wheels. A control law computes commands for the reaction wheels in terms of the desired two-axis fine pointing spacecraft torques and TAG gimbal angles to reduce the pointing errors and to minimize the sum of squares of the reaction-wheel torques. The minimization of sum of squares has the effect of minimizing the reaction-wheel power required by causing the wheel having its spin axis closest to the desired fine pointing axis to be driven the hardest.

Interaction between the simultaneously operating fine pointing and coarse pointing control laws is not a problem because the coarse pointing time constants are chosen to be much lower than those of the fine pointing law.

Energy storage.- Electrical power functions to be performed by the TAG system include the storage and regeneration of the electrical energy required by the spacecraft and its payload. Solar arrays (see fig. 4) generate power for the spacecraft and payload and for accelerating the energy wheels during the orbital day. The energy-wheel generators return the stored energy to the spacecraft during the orbital night. The flight

computer manages the power transfer and maintains equal spin rates for the energy wheels. The torque on the spacecraft caused by power transfer is counteracted automatically by controlled precession of the gimbals.

Control system desaturation.- The spin rates of the reaction wheels are maintained near zero to minimize the power required and to maximize their dynamic range. This condition is accomplished by feeding back each reaction-wheel speed in its corresponding torque control law. The torque caused by this desaturation is counteracted by driving the TAG gimbals and results in an equal and opposite precession torque on the spacecraft.

TAG system momentum accumulation due to gravity gradient and aerodynamic bias torques on the spacecraft is controlled by using an electromagnetic torquer acting in the Earth's magnetic field. A magnetometer is used to sense the Earth's magnetic flux direction with respect to the spacecraft. These data are transferred to the flight computer along with measured TAG momentum levels and gimbal angles. Appropriate currents are computed and induced in the magnetic coils to produce the required torques on the spacecraft.

TAG and Spacecraft Control Laws

In this section the control laws for the spacecraft and the TAG system are formulated and discussed.

Coarse pointing control law.- The spacecraft coarse pointing control law computes the three-axis control torques required to hold the spacecraft within specified coarse pointing limits. It is the only source of spacecraft roll control. For this study a typical linear law is assumed that gives the desired x_S, y_S, and z_S body-axis control torques in terms of the measured body-axis attitude and angular rate errors with respect to inertial space. This control law is defined by the following relation:

$$\underline{T}_{CD} \triangleq K_{AC}\underline{\theta}_C + K_{RC}\underline{\Omega}_C \tag{5}$$

where $\underline{\theta}_C$ and $\underline{\Omega}_C$ are the measured coarse pointing attitude and angular rate errors, respectively, and have the form

$$\underline{\theta}_C = \begin{bmatrix} \phi_C & \theta_C & \psi_C \end{bmatrix}^T$$

$$\underline{\Omega}_C = \begin{bmatrix} p_C & q_C & r_C \end{bmatrix}^T$$

The attitude and rate gains for the control law depend on the spacecraft mass properties and mission coarse pointing and damping requirements. The gains are expressed in matrix form as

$$K_{AC} = \text{diag}\begin{pmatrix} K_{ACx} & K_{ACy} & K_{ACz} \end{pmatrix}$$

$$K_{RC} = \text{diag}\begin{pmatrix} K_{RCx} & K_{RCy} & K_{RCz} \end{pmatrix}$$

The method used for computing the elements of the gain matrices is discussed in appendix B. Equation (5) is used as input to the gimbal rate control law.

Fine pointing control law.- The fine pointing control law computes the spacecraft y_S and z_S body-axis control torques required to hold the spacecraft within specified fine pointing error limits. The control law is linear and is defined as

$$\underline{T}_{FD} \triangleq K_{AF}\underline{\theta}_F + K_{RF}\underline{\Omega}_F \tag{6}$$

where $\underline{\theta}_F$ and $\underline{\Omega}_F$ are the measured fine pointing attitude and angular rate errors, respectively, and are given by

$$\underline{\theta}_F = \begin{bmatrix} \theta_F & \psi_F \end{bmatrix}^F$$

$$\underline{\Omega}_F = \begin{bmatrix} q_F & r_F \end{bmatrix}^T$$

The fine pointing attitude and rate gains are given by

$$K_{AF} = \text{diag}\begin{pmatrix} K_{AFy} & K_{AFz} \end{pmatrix}$$

$$K_{RF} = \text{diag}\begin{pmatrix} K_{RFy} & K_{RFz} \end{pmatrix}$$

The individual attitude and rate gains are selected to give the required pointing accuracy and damping. Equation (6) is used as input to the reaction-wheel control law.

Reorientation control law.- The spacecraft reorientation control law computes command torques about the three spacecraft axes in terms of measured and commanded angular rates. The commanded rates are mission and spacecraft dependent but are on the order of 6°/min. The reorientation control law used in this study is defined by the following relation:

$$\underline{T}_{MD} \triangleq K_{RM}\left\{\underline{\Omega}_M - \underline{\Omega}_{MD}\right\} \tag{7}$$

where $\underline{\Omega}_M$ and $\underline{\Omega}_{MD}$ are the measured and desired angular rate vectors, respectively. These vectors are given in terms of desired and measured body rates as

$$\underline{\Omega}_{MD} = \begin{bmatrix} p_{MD} & q_{MD} & r_{MD} \end{bmatrix}^T$$

$$\underline{\Omega}_{M} = \begin{bmatrix} p_{M} & q_{M} & r_{M} \end{bmatrix}^T$$

The maneuver rate gains depend on angular acceleration requirements and are given by

$$K_{RM} = \text{diag}\begin{pmatrix} K_{RMx} & K_{RMy} & K_{RMz} \end{pmatrix}$$

Equation (7) is used as input to the gimbal rate control law.

The fine and coarse pointing control laws are deactivated during reorientations and are reactivated only when the spacecraft attitude is within the range of the coarse pointing sensors. Particular details of the reorientation logic are not considered pertinent to this analysis and are omitted. The reader is referred to references 7 and 14 for further details.

Gimbal rate control law.- The gimbal rate control law determines the gimbal rate commands that will produce the desired torques for spacecraft coarse pointing, reorientation, reaction-wheel desaturation, and cancellation of the energy-wheel torque, while simultaneously minimizing functions of the gimbal angles and rates. Before this control law can be formulated, the torque equation for the TAG system must be developed.

The torque applied to a spacecraft by a TAG unit, due to gimbal motion, spacecraft angular motion, and wheel acceleration is given by equation (1). For the system of n units the net torque applied to the spacecraft is equal to the vector sum of the individual torques given as

$$\underline{T}_T = \sum_{i=1}^{n} \underline{T}_U^i \tag{8}$$

where the superscript i replaces the superscript S of equation (1) and denotes the ith TAG unit in the system.

In this analysis it is assumed, because of the high angular momentum of the energy wheels, that the total angular momentum for each TAG unit $\underline{H}_T^i$ given by equation (2) is equal to the energy-wheel momentum alone given by the expression

$$\underline{H}^i = H_i \begin{Bmatrix} -s\beta_i \\ c\alpha_i c\beta_i \\ s\alpha_i c\beta_i \end{Bmatrix} \tag{9}$$

Here H_i is the energy-wheel momentum $I_{HA}\omega_{Hi}$, and α_i and β_i are the outer and inner gimbal angles, respectively, for the ith TAG unit.

Substituting equation (9) into equation (1), with the appropriate superscripts, and using equation (8), the expression for the torque $\underline{T}_T$ on the spacecraft can be written as

$$\underline{T}_T = \Gamma\tilde{H}\dot{\underline{\gamma}} - [\Omega]R\underline{H} - R\dot{\underline{H}} \tag{10}$$

where Γ is a 3 by 2n matrix expressed as

$$\Gamma = \begin{bmatrix} 0 & \cdots & 0 & c\beta_1 & \cdots & c\beta_n \\ c\beta_1 s\alpha_1 & \cdots & c\beta_n s\alpha_n & s\beta_1 c\alpha_1 & \cdots & s\beta_n c\alpha_n \\ -c\beta_1 c\alpha_1 & \cdots & -c\beta_n c\alpha_n & s\beta_1 s\alpha_1 & \cdots & s\beta_n s\alpha_n \end{bmatrix} \tag{11}$$

and $\dot{\underline{\gamma}}$, the relative gimbal rate vector, is given by

$$\dot{\underline{\gamma}} = \begin{bmatrix} \dot{\alpha}_i & \cdots & \dot{\alpha}_n & \dot{\beta}_1 & \cdots & \dot{\beta}_n \end{bmatrix}^T$$

The spin momentum magnitude matrix $\tilde{H}$ is given as

$$\tilde{H} = \text{diag}\begin{pmatrix} H_1 & \cdots & H_n & H_1 & \cdots & H_n \end{pmatrix}$$

The skew symmetric matrix $[\Omega]$ is the spacecraft angular rate cross-product matrix. The vector $R\underline{H}$ is the total TAG system spin momentum expressed in spacecraft coordinates where the transformation matrix R is given by

$$R = \begin{bmatrix} -s\beta_1 & \cdots & -s\beta_n \\ c\alpha_1 c\beta_1 & \cdots & c\alpha_n c\beta_n \\ s\alpha_1 c\beta_1 & \cdots & s\alpha_n c\beta_n \end{bmatrix} \tag{12}$$

and the spin momentum column matrix $\underline{H}$ is given by

$$\underline{H} = \begin{bmatrix} H_1 & \cdots & H_n \end{bmatrix}^T$$

The last term of equation (10) represents the torques on the spacecraft due to wheel acceleration where

$$\dot{\underline{H}} = \begin{bmatrix} \dot{H}_1 & \cdots & \dot{H}_n \end{bmatrix}^T$$

The energy-wheel speeds are controlled so that they are equal at all times. Thus, a further simplifying assumption can be made. The individual momentum magnitudes of the TAG units are assumed to be equal to the average value so that the matrix $\tilde{H}$ defined previously can be replaced by the scalar H given by

$$H = \frac{1}{n} \sum_{i=1}^{n} I_{HA}\omega_{Hi} \tag{13}$$

The first two terms on the right-hand side of equation (10) represent the torque $\underline{T}_P$ on the spacecraft due to gimbal motion and angular motion of the spacecraft, and is given as

$$\underline{T}_P = H\Gamma\dot{\underline{\gamma}} - [\Omega]R\underline{H} \tag{14}$$

The remaining term in equation (10) gives the torque $\underline{T}_A$ on the spacecraft due to reaction-wheel and energy-wheel acceleration, and is given by

$$\underline{T}_A = -R\dot{\underline{H}} \tag{15}$$

By considering the spacecraft torque requirements and the torque equation (14), the desired precession torque $\underline{T}_G$ is defined in spacecraft coordinates as

$$\underline{T}_G \triangleq (1 - m)\underline{T}_{CD} + m\left(\underline{T}_{MD} + [\Omega]R\underline{H}\right) - K_R R\underline{\omega}_L + R\underline{T}_{HC} \tag{16}$$

where $m = 1$ for reorientation and $m = 0$ for pointing. The command torques $\underline{T}_{CD}$ and $\underline{T}_{MD}$ are given by equations (5) and (7). The term $[\Omega]R\underline{H}$ cancels the TAG torque on the spacecraft due to the spacecraft angular rate during reorientations. (The elements of $[\Omega]$, R, and $\underline{H}$ are obtained from measurements.) The third term in equation (16) cancels the reaction-wheel speed desaturation torque. The measured reaction-wheel speeds are given in matrix form by

$$\underline{\omega}_L = \left[\omega_{L1} \cdots \omega_{Ln}\right]^T$$

The scalar K_R is the desaturation gain, and the matrix R, transforms $\underline{\omega}_L$ to spacecraft coordinates. The last term in equation (16) cancels the energy transfer torque. The matrix of energy-wheel torque commands is given by

$$\underline{T}_{HC} = \left[T_{HC1} \cdots T_{HCn}\right]^T$$

and is derived later. The matrix R transforms $\underline{T}_{HC}$ into spacecraft coordinates.

The gimbal rate control law is based on setting the desired torque $\underline{T}_G$, defined by equation (16), equal to the expression for the TAG precession torque $H\Gamma\dot{\underline{\gamma}}$ with a subscript D given to $\dot{\underline{\gamma}}$ to denote the desired value. This relation is expressed as

$$\underline{T}_G = H\Gamma\dot{\underline{\gamma}}_D \tag{17}$$

To obtain the control law, equation (17) is solved for $\dot{\underline{\gamma}}_D$ in terms of $\underline{T}_G$. Equation (17) represents three equations in 2n unknowns; therefore, 2n - 3 additional equations are needed to solve for $\dot{\underline{\gamma}}_D$. The method used to obtain the additional equations is similar to one derived by S. C. Chu and J. Kranton.

Equation (17) is taken as a constraint, and a function to be minimized is developed to obtain the additional equations necessary to solve for $\dot{\underline{\gamma}}_D$. The function to be minimized is now formulated.

It is desirable to keep the gimbals as close as possible to their reference position because with a redundant system there is no unique set of gimbal angles for a given total angular momentum. This nonuniqueness allows gimbal drift which usually results in one or more gimbals encountering mechanical stops or, in systems without stops, inner gimbal angles approaching $\pm 90^{\circ}$; both conditions are to be avoided. Furthermore, minimum rate control laws in redundant systems tend to cause gimbal drift that can result in loss of control. For example, in a three CMG system if two parallel momentum vectors oppose the third, loss of control about the mutual axis is experienced.

In the present study 2n functions are defined that give a measure of the gimbal travel from the reference positions. The ith outer gimbal function is defined as

$$f_i(\alpha_i) \triangleq F_A\left(1 - \cos(\alpha_i - \alpha_{iO})\right) \operatorname{sgn}\left(-\sin(\alpha_i - \alpha_{iO})\right) \tag{18}$$

and the ith inner gimbal function is defined by

$$f_{n+i}(\beta_i) \triangleq F_B(1 - \cos\beta_i) \operatorname{sgn}\left(-\sin\beta_i\right) \tag{19}$$

These functions are zero when the gimbals are in their reference positions. The outer gimbal functions vary as $1 - \cos(\alpha_i - \alpha_{iO})$ to a value of $2F_A$ at $\alpha_i - \alpha_{iO} = \pm 180^{\circ}$, and the inner gimbal functions vary as $1 - \cos\beta_i$ to a value of $2F_B$ at $\beta_i = \pm 180^{\circ}$. The signum term causes the functions to have the sign opposite to $\alpha_i - \alpha_{iO}$ and β_i. Part of the function to be minimized is taken as the sum of squares of the gimbal angle functions given by equations (18) and (19).

The second part of the function to be minimized is formed by realizing that at each instant of time, certain gimbals are better suited to produce the desired control torque because of lower rate requirement. This condition suggests that minimizing the sum of

squares of command gimbal rates would cause the most favorable gimbals to be used. This particular minimization has the effect of minimizing the gimbal power required.

With these considerations the scalar function J_p to be minimized is defined as

$$J_p \triangleq \frac{1}{2}\left[\dot{\underline{\gamma}}_D^T + \underline{f}^T(\gamma)\right] Q \left\{\dot{\underline{\gamma}}_D + \underline{f}(\gamma)\right\}$$

where $\dot{\underline{\gamma}}_D$ is the matrix of desired gimbal rates, and $\underline{f}(\gamma)$ is the 2n by 1 matrix of specified functions of the gimbal angles given in equations (18) and (19). The constant matrix Q is a 2n by 2n diagonal weighting matrix which is used to weight inner gimbal rates against the outer gimbal rates. For equal weighting Q is an identity matrix.

To solve for the command gimbal rates that will satisfy equation (17) and at the same time minimize the function J_p, a three vector of Lagrange multipliers $\underline{\lambda}$ is introduced and the new function J_p^* to be minimized is formed as

$$J_p^* = \frac{1}{2}\left[\dot{\underline{\gamma}}_D^T + \underline{f}^T(\gamma)\right] Q \left\{\dot{\underline{\gamma}}_D + \underline{f}(\gamma)\right\} + \underline{\lambda}^T \left\{\Gamma \dot{\underline{\gamma}}_D - \frac{1}{H}\underline{T}_G\right\}$$

Since J_p is a positive definite function, the necessary and sufficient condition for a minimum of J_p^* is that the partial derivatives of J_p^* with respect to the elements of $\dot{\underline{\gamma}}_D$ all be zero. Omitting the details of this derivation, the result is given as

$$\dot{\underline{\gamma}}_D = -\underline{f}(\gamma) + Q^{-1}\Gamma^T\left(\Gamma Q^{-1}\Gamma^T\right)^{-1}\left(\frac{1}{H}\underline{T}_G + \Gamma \underline{f}(\gamma)\right) \tag{20}$$

Equation (20) gives the gimbal rate commands in terms of the desired torque $\underline{T}_G$, the gimbal rate weighting matrix Q, the gimbal angle coefficient matrix Γ, the average angular momentum magnitude H of all TAG units, and the desired gimbal angle functions $\underline{f}(\gamma)$. The matrix $\Gamma Q^{-1}\Gamma^T$ is a 3 by 3 matrix which must be inverted in real time. The elements of $\Gamma Q^{-1}\Gamma^T$ are trigonometric functions of the gimbal angles which do not vary rapidly; therefore, the inversion frequency can be relatively low, on the order of once per second.

Reaction-wheel control law.- The reaction-wheel control law for the TAG system is derived in this section. The purpose of this control law is to determine reaction-wheel commands that will produce the fine pointing control torques given by equation (6).

The reaction on the spacecraft resulting from torques applied to the reaction wheels is given in spacecraft axes by the following expression:

$$\underline{T}_{LS} = -R\underline{T}_L \tag{21}$$

where R is the transformation matrix given by equation (12), and the torques applied to the reaction wheels are given in matrix form as

$$\underline{T}_L = \left[T_{L1} \cdot \cdot \cdot T_{Ln}\right]^T$$

For this study $\underline{T}_{LS}$ is the contribution of the reaction wheels to $\underline{T}_A$ given earlier by equation (15).

For the derivation, the spacecraft torque $\underline{T}_{LS}$ is replaced by the desired two-axis fine pointing torque $\underline{T}_{FD}$ given by equation (6). The reaction-wheel torque $\underline{T}_L$ is given the subscript D to denote the desired value, and the first row of R is deleted for compatibility. This relationship gives

$$\underline{T}_{FD} = -\tilde{R}\underline{T}_{LD} \tag{22}$$

where

$$\tilde{R} = \begin{bmatrix} c\alpha_1 c\beta_1 \cdot \cdot \cdot c\alpha_n c\beta_n \\ s\alpha_1 c\beta_1 \cdot \cdot \cdot s\alpha_n c\beta_n \end{bmatrix} \tag{23}$$

and

$$\underline{T}_{LD} = \left[T_{LD1} \cdot \cdot \cdot T_{LDn}\right]^T$$

To obtain the control law, equation (22) must be solved for $\underline{T}_{LD}$ in terms of $\underline{T}_{FD}$. The matrix $\tilde{R}$ is 2 by n and direct solutions of equation (22) for $\underline{T}_{LD}$ can be obtained only when $n = 2$ and $\tilde{R}^{-1}$ exists. Since $n \geq 2$ for the TAG system considered here, additional equations are needed for the case where $n > 2$.

The same general method that was used to derive the gimbal rate control law is used in this case. Equation (22) is considered as an equation of constraint, and a scalar function J_R to be minimized is defined as

$$J_R \triangleq \frac{1}{2}\underline{T}_{LD}^T\underline{T}_{LD} \tag{24}$$

Here J_R is the sum of squares of the desired reaction-wheel torques and is a measure of the power required by the reaction wheels. To determine the reaction-wheel torque commands that will satisfy equation (22) and minimize J_R, a three vector of Lagrange multipliers $\underline{\lambda}$ is introduced and a new function J_R^* to be minimized is formed as

$$J_R^* = \frac{1}{2}\underline{T}_{LD}^T\underline{T}_{LD} + \underline{\lambda}^T\left(\tilde{R}\underline{T}_{LD} + \underline{T}_{FD}\right)$$

As before J_R is a positive definite function so the necessary and sufficient condition for a minimum of J_R^* is that partial derivatives with respect to the elements of $\underline{T}_{LD}$ all be zero. Taking the required partial derivatives and solving for $\underline{T}_{LD}$ gives

$$\underline{T}_{LD} = -\tilde{R}^T\left(\tilde{R}\tilde{R}^T\right)^{-1}\underline{T}_{FD} \tag{25}$$

Equation (25) gives part of the reaction-wheel commands in terms of the desired fine pointing torque $\underline{T}_{FD}$ given in equation (6) and the transformation matrix $\tilde{R}$ given in equation (23). The matrix $\tilde{R}\tilde{R}^T$ is a 2 by 2 matrix which is inverted in real time. The elements of the matrix vary slowly and the inversion frequency need not be high. A closed form solution for $\tilde{R}^T\left(\tilde{R}\tilde{R}^T\right)^{-1}$ is given in appendix C in equation (C5) for the case where $n = 3$.

Reaction-wheel desaturation is accomplished by adding the term $-K_R\underline{\omega}_L$ to equation (25) to form the total reaction-wheel torque command as

$$\underline{T}_{LD} = -\tilde{R}^T\left(\tilde{R}\tilde{R}^T\right)^{-1}\underline{T}_{FD} - K_R\underline{\omega}_L \tag{26}$$

where K_R is the desaturation gain and $\underline{\omega}_L$ is the matrix of reaction-wheel speeds. To verify that equation (26) produces the desired fine pointing torque, it is substituted into equation (21) to get

$$\underline{T}_{LS} = R\tilde{R}^T\left(\tilde{R}\tilde{R}^T\right)^{-1}\underline{T}_{FD} + RK_R\underline{\omega}_L \tag{27}$$

If the definition of R is recalled, the first term of equation (27) gives the required two-axis torque exactly, but it also may produce a torque about the roll axis of the spacecraft unless all inner gimbal angles are equal to zero. This torque will cause some error about the roll axis, but the coarse pointing control law will minimize it. The second term in equation (26) produces the torque required to keep the reaction-wheel speeds sufficiently low. An equal and opposite torque is applied to the spacecraft by the gimbal rate control law so that there is no net torque applied to the spacecraft as a result of the reaction-wheel desaturation.

Energy storage control law.- The TAG system energy storage control law is formulated in this section. The purpose of the control law is to provide commands for the energy-wheel motor generators to effect the required electrical power transfer and to maintain equal energy-wheel speeds. For the control law derivation it is assumed that the energy-wheel electrical power is equal to the mechanical power given by the relation

$$P_T = \sum_{i=1}^{n} \omega_{Hi} T_{Hi} \tag{28}$$

where ω_{Hi} is the ith wheel speed, and T_{Hi} is the ith motor-generator torque. The control law must give the value of T_{Hi} required to produce P_T and keep the ω_{Hi} equal.

To derive the control law, an energy error function for the ith energy wheel is defined in terms of the total TAG system kinetic energy as

$$\epsilon_i \triangleq \frac{1}{2} I_{HA} \omega_{Hi}^2 - \frac{E_T}{n} \tag{29}$$

where the energy E_T is given by

$$E_T = \frac{1}{2} I_{HA} \underline{\omega}_H^T \underline{\omega}_H \tag{30}$$

and I_{HA} is the energy-wheel spin moment of inertia. The control law is obtained by letting the time derivative of the error ϵ_i be proportional to its negative as

$$\dot{\epsilon}_i = -\frac{1}{k} \epsilon_i \tag{31}$$

This requirement causes each ω_{Hi} to approach $\sqrt{\frac{2E_T}{nI_{HA}}}$ with time constant k seconds.

Using $I_{HA}\dot{\omega}_{Hi} = T_{Hi}$ and $\dot{E}_T = P_T$ with equations (29), (30), and (31) and letting $T_{HCi} = T_{Hi}$ represent the ith energy-wheel command gives

$$T_{HCi} = \frac{1}{\omega_{Hi}} \left[\frac{P_T(t)}{n} - \frac{1}{k}\left(\frac{1}{2} I_{HA} \omega_{Hi}^2 - \frac{E_T}{n} \right) \right] \tag{32}$$

as the ith energy-wheel torque control law. Implementation of this control law requires continuous measurement of ω_{Hi} and P_T and computation of E_T.

Magnetic torquer control law.- The magnetic torquer control law for TAG momentum management is developed in this section. The result is similar to that of Levidow. The torque $\underline{T}_B$ acting on a spacecraft due to an attached magnet of magnetic moment $\underline{M}$ is given by the following relation:

$$\underline{T}_B = -[\underline{B}]\underline{M} \tag{33}$$

where $\underline{B}$ is the flux density of the Earth's magnetic field, and $[\underline{B}]$ is the matrix equivalent to the vector cross-product operation. Equation (33) indicates that the torque on the spacecraft is perpendicular to both $\underline{M}$ and $\underline{B}$, and that torque cannot be generated in a direction parallel to the Earth's magnetic field $\underline{B}$. Because $\underline{B}$ depends entirely on the location of the spacecraft in orbit, $\underline{T}_B$ can be controlled only by changing the magnitude and/or direction of $\underline{M}$. Since the torque generated will always be perpendicular to $\underline{B}$, the direction of $\underline{T}_B$ cannot be completely controlled. To resolve this problem, a control law that effects a net reduction of accumulated system momentum each orbit is found by determining $\underline{M}(t)$ so that the following relation holds:

$$\underline{H}_b = \int_0^{T_O} [\underline{B}(\tau)]\underline{M}(\tau)d\tau \tag{34}$$

where $\underline{H}_b$ is the momentum to be dumped in one orbit period T_O. There are an infinite number of functions $\underline{M}(t)$ that will satisfy equation (34). Optimization techniques are used to choose the $\underline{M}(t)$ that minimizes the magnet energy required. The magnitude of $\underline{M}$ is directly related to electrical power required; therefore, an energy cost functional J_M is defined as

$$J_M = \frac{1}{2}\int_0^{T_O} \underline{M}^T\underline{M}\, d\tau$$

This problem now has the form of the isoperimetric problem of the calculus of variations (see section 12 of ch. 2 in ref. 15) where the vector function $\underline{M}(t)$ is to be found that minimizes the functional J_M subject to the three functional constraints given by equation (34). For this case the necessary condition for an extremum is that

$$\frac{\partial}{\partial M_i}\left(\frac{1}{2}\underline{M}^T\underline{M} + \underline{\lambda}[\underline{B}]\underline{M}\right) = 0 \qquad (i = 1, 2, 3)$$

where $\underline{\lambda}$ is a three vector of constant Lagrange multipliers. Performing the differentiation and using equation (34) gives the control law as

$$\underline{M}(t) = [\underline{B}(t)]\left(\left\{\int_0^{T_O} [\underline{B}(\tau)]^2 d\tau\right\}^{-1} \underline{H}_b\right) \tag{35}$$

Equation (35) represents the cross product of the vector $\underline{B}(t)$ with the constant vector enclosed in the braces. Implementation of equation (35) requires a once-per-orbit computation of the vector in braces and continuous real-time multiplication by $[\underline{B}(t)]$ to get $\underline{M}(t)$. The elements of the matrix $[\underline{B}(t)]$ are continuously measured by magnetometers attached to the spacecraft. The elements of the matrix $[\underline{B}(\tau)]$ are determined in advance for a complete orbit based on estimated orbit parameters and orientation of the spacecraft. The bias momentum $\underline{H}_b$ is equal to the residual bias momentum from

previous orbits plus the estimated bias momentum for the next orbit. The vector function $\underline{M}(t)$ is used as a continuous control command input to the electromagnetic controller and it is updated each orbit.

SYSTEM EVALUATION

The basic TAG system and its associated control laws having been defined, it now becomes necessary to evaluate the performance of the system in the spacecraft control loop. In addition, it is deemed necessary to determine whether the multifunction capability of the TAG system will be detrimental to its control and energy transfer effectiveness.

Example Mission Description

To conduct the TAG system evaluation, a candidate mission with stringent pointing, stability, and moderate energy storage requirements has been selected. The spacecraft chosen is representative of a class of low-Earth-orbit spacecraft which have been designated as shuttle-launched research and applications modules (RAMs). The particular mission selected is an advanced solar observatory, RAM A303B, shown in figure 6. The spacecraft and mission requirements for a growth version of the RAM A303B were generated by the RAM study. The inertias associated with the selected vehicle are given as

$$I_S = \text{diag}\,(40\,600 \quad 406\,000 \quad 406\,000)\ \text{kg-m}^2 \tag{36}$$

The spacecraft operates in a 279-km circular orbit at an inclination of 55° with an orbit period of 90 minutes. The vehicle is maintained in a solar orientation with its minimum axis of inertia (x_S) pointed toward the Sun.

The attitude control requirements, summarized in table I, for this mission are 1 arc second pointing accuracy with 0.017 arc second pointing stability about the y_S- and z_S-axis during a 45-minute observation period. The x_S-axis is to be stabilized to 5 arc seconds. Minimum momentum storage requirements for the spacecraft resulting from orbit disturbances and slewing requirements are estimated to be 2034 N-m-sec. No crew disturbances are considered in these estimates since the vehicle is unmanned, except during periods of revisit and servicing.

Using the same ground rules as established for the baseline system of the RAM study, the TAG system must provide full control as well as 85 percent of the nominal energy storage capability or 2.2 kW-hr with one unit failed. The high-speed wheels of the TAG units are sized primarily from energy considerations. The momentum level is maintained at a minimum by operating at as high a rotor speed as material and component physical characteristics will permit.

RAM-TAG System Description

The TAG system configuration selected for evaluation is comprised of three TAG units with the outer gimbal axes parallel to the x_S-axis. The system is initially in a zero-momentum reference configuration as depicted in figure 7.

By using the results of the IPACS study, the TAG energy wheel operates at a maximum speed of 45 000 rpm and has a spin moment of inertia $I_{HA} = 0.48$ kg-m^2. This condition results in an angular momentum capacity of 2247 N-m-sec at full speed and an energy storage capacity of 1.1 kW-hr over a speed reduction range of 50 percent.

From the power profile shown in figure 8, it has been calculated that the maximum torque resulting from a large power demand is 1.02 N-m per wheel at 50-percent speed. The maximum torque applied to the vehicle during the charging cycle of the energy wheel has been estimated at 0.66 N-m at 50-percent speed.

The reaction wheels for the TAG system exhibit the same performance characteristics as the reaction wheels of the RAM study baseline systems. These wheels possess a spin moment of inertia $I_{LA} = 0.45$ kg-m^2 and operate at a maximum speed of 85 rpm resulting in a momentum capacity of 4 N-m-sec.

The constants in the TAG system control laws for the example RAM spacecraft and mission simulation are derived in appendix B. These constants are summarized herein.

The coarse pointing and fine pointing attitude gain matrices K_{AC} and K_{AF} and attitude rate gain matrices K_{RC} and K_{RF} used in equations (5) and (6) are given as

$$K_{AC} = \text{diag}\left(-8.23 \times 10^4 - 1.13 \times 10^6 - 1.13 \times 10^6\right) \text{N-m/rad}$$
$$K_{AF} = \text{diag}\left(-3.32 \times 10^7 - 3.32 \times 10^7\right) \text{N-m/rad}$$
$$K_{RC} = \text{diag}\left(-8.09 \times 10^5 - 9.48 \times 10^5 - 9.48 \times 10^5\right) \text{N-m/(rad/sec)}$$
$$K_{RF} = \text{diag}\left(-5.14 \times 10^6 - 5.14 \times 10^6\right) \text{N-m/(rad/sec)}$$

respectively.

The reaction-wheel desaturation gain K_R used in equations (16) and (26) is given as $K_R = 0.308$ N-m/(rad/sec). The energy-wheel time constant k used in equation (32) has the value $k = 360$ seconds. The constants F_A and F_B in the gimbal angle function $f(\underline{\gamma})$ given by equations (18) and (19) are given as

$$F_A = 0.0111 \text{ (rad/sec)/rad}$$

$$F_B = 0.0222 \text{ (rad/sec)/rad}$$

The weighting matrix Q used in the gimbal rate control law given by equation (20) is taken as the identity matrix for this study.

Simulation Results

In this section the results of the RAM-TAG system computer simulation are presented. See figures 9 and 10 and appendix C for a description of the simulation. The various control laws discussed earlier are considered separately, where possible, to verify their operation in the system. The complete system is then considered to evaluate its performance over one orbit period. Finally, reorientation rate acquisitions are discussed.

Effect of the functions $\underline{f}(\gamma)$.- Figures 11 and 12 show the effect of the gimbal angle functions $\underline{f}(\gamma)$ given by equations (18) and (19) for two different sets of initial gimbal angles. In both cases there are no gravity-gradient torques nor power-transfer torques included. The energy wheels have equal spin rates at 25 000 rpm. The time scales shown are 1 minute per division. In figure 11 the outer gimbals are initially 90° from their reference position so that $\alpha_1 = 90^{\circ}$, $\alpha_2 = 210^{\circ}$, and $\alpha_3 = -30^{\circ}$; the inner gimbal angles have the values $\beta_1 = 45^{\circ}$, $\beta_2 = -45^{\circ}$, and $\beta_3 = 0^{\circ}$. The components of total momentum initially are computed (based on a per wheel momentum H of 1250 N-m-sec) as

$$\underline{RH} = \begin{Bmatrix} 0 \\ 317 \\ -183 \end{Bmatrix} \text{ N-m-sec}$$

After 26 minutes of simulation, the total momentum is computed as

$$\underline{RH} = \begin{Bmatrix} 0 \\ 309 \\ -197 \end{Bmatrix} \text{ N-m-sec}$$

by using gimbal angles of $\alpha_1 = -6^{\circ}$, $\alpha_2 = 116^{\circ}$, $\alpha_3 = -108^{\circ}$, $\beta_1 = 2^{\circ}$, $\beta_2 = -4^{\circ}$, and $\beta_3 = 2^{\circ}$. Theoretically, the two values of $\underline{RH}$ should be the same; inaccuracy in reading the final values of the gimbal angles is thought to be the cause of the difference. Spacecraft pointing errors were monitored during this case and were found to be less than 0.1 arc second in roll and less than 0.01 arc second in pitch and yaw.

Figure 12 shows the gimbal motion when initially $\alpha_1 = 0^{\circ}$, $\alpha_2 = 176^{\circ}$, $\alpha_3 = -176^{\circ}$ and $\beta_i = 0^{\circ}$ $(i = 1, 2, 3)$. This orientation is considered as a "semi" worst case in that precession control torques are difficult to produce about the y_S-axis since the three

momenta lie close to the y_S-axis. It is found in the simultations that if α_2 and α_3 are any closer to 180^o initially, then control is lost. This initial gimbal orientation gives a total angular momentum of

$$\underline{RH} = \begin{Bmatrix} 0 \\ -1247 \\ 0 \end{Bmatrix} \text{ N-m-sec}$$

After 20 minutes of simulation the gimbals had reached steady states at $\alpha_1 = -24^o$, $\alpha_2 = 152^o$, $\alpha_3 = -176^o$, $\beta_1 = 26^o$, $\beta_2 = -12^o$, and $\beta_3 = -12^o$. These data give the total momentum as

$$\underline{RH} = \begin{Bmatrix} -28 \\ -1272 \\ 31 \end{Bmatrix} \text{ N-m-sec}$$

The change in total momentum is again due to inaccuracy in reading the final gimbal angles. Spacecraft motion during this case remained stable at levels below 1.0 arc seconds in roll and below 0.1 arc second in pitch and yaw.

Effect of reaction-wheel speed feedback.- Figures 13 and 14 show the effect of the reaction-wheel speed feedback in equation (26). In figure 13 the outer gimbal angles are in their reference positions and all the inner gimbals are at 60^o. There are no external disturbance torques applied to the spacecraft, and the energy wheels each have spin rates of 25 000 rpm. The time scale is 1 second per division. Initial reaction-wheel speeds of 50 rpm are used. The figure shows the reaction-wheel speed time histories and the spacecraft angular errors for a time of approximately 17 seconds. The wheel-speed time to damp to half-amplitude is seen to be approximately 1 second. No detectable pointing error is caused in pitch (θ) and yaw (ψ) and approximately 0.4 arc second error is caused in roll (ϕ). The roll-angle errors that appear at approximately 10 and 15 seconds are due to the loss of roll control every 5 seconds during the 460 msec control computation. These errors are far below the allowable 5 arc seconds.

Figure 14 shows the results of having $\omega_{L1} = 100$ rpm and $\omega_{L2} = \omega_{L3} = 0$ rpm initially. Here all gimbals are in their reference positions. The energy wheels each have spin rates of 25 000 rpm. The time scale is 1 second per division. In this case all the excess reaction-wheel momentum is along the spacecraft y_S-axis. During the desaturation a pointing error of approximately 0.005 arc second about the y_S-axis occurs. Outer gimbals 2 and 3 are seen to rotate about 0.1^o to compensate for the change

in angular momentum. Similar cases were run for the other two wheels and the results were comparable to this case.

Effect of energy-wheel speed control.- Figure 15 shows the effect of the energy-wheel speed control law given by equation (32). In this case ω_{H1} = 25 000 rpm and $\omega_{H2} = \omega_{H3}$ = 35 000 rpm. All gimbals are in their reference positions initially, and there are no gravity-gradient nor power-transfer torques acting on the spacecraft. The time scale is 1 minute per division. The simulation is run for 12 to 13 minutes. The wheel speeds equalize in approximately 6 minutes (the time constant k). The outer gimbals 2 and 3 rotate to compensate for the changing momentum to $\alpha_2 = 130^o$ and $\alpha_3 = -130^o$.

Effect of impulsive torque distrubances.- Figure 16 shows the effect of an impulsive torque of 2 N-m-sec applied about the spacecraft y_S-axis. The 2 N-m-sec level was chosen to cause the reaction-wheel torque motors to saturate. Here all gimbals are in their reference positions initially. The energy wheels have spin rates of 25 000 rpm and there are no gravity-gradient nor power-transfer torques applied. A y_S-axis pointing error of 0.18 arc second is caused. The ensuing motion shows that command torque limiting (set at 4 N-m per axis) occurred during the first 0.7 second of motion. This value is determined by noting the initial straight-line segments in the reaction-wheels' time histories. The reaction-wheel speeds returned to zero because of the desaturation scheme. The slight offset is due to computational inaccuracies. The same impulse magnitude was applied about the z_S-axis and comparable response was obtained.

Effect of constant torque disturbance.- Figure 17 shows the effect of a constant torque applied about the roll axis of the spacecraft. The magnitude of the disturbance torque is 2.74 N-m equal to the maximum power transfer torque of 2 N-m plus the maximum gravity-gradient torque of 0.74 N-m. The gimbals are in the reference positions and the energy wheels have spin rates of 25 000 rpm. The time scale in the figure is 1 second per division. The theoretical pointing error caused by the 2.74 N-m disturbance is computed to be 6.72 arc seconds. The simulation gives approximately this value. The roll damping is seen to be close to the desired 0.7 value. The inner gimbals are used to control the spacecraft in this case and their time histories are shown in the figure. In this case the pitch and yaw pointing errors remained below 0.005 arc second.

Figure 18 shows the effect of the constant 2.74 N-m torque applied about the spacecraft y_S-axis. All other conditions are the same as in the previous case. The theoretical pointing error caused by the 2.74 N-m torque is 0.017 arc second. The simulation pointing error is close to this value as is seen in the figure. The reaction-wheels' responses are shown on the right-hand side of the figure, and it is seen that reaction-wheel speeds level off as desired. It is noted that this maximum disturbance torque causes a maximum speed of 10 rpm where the units are designed for 85 rpm. Time

histories for outer gimbals 2 and 3 are shown on the left-hand side of the figure, and it is seen that these gimbals control the reaction-wheel speeds while the reaction wheels control the spacecraft. This case was also run for the z_S-axis and the results were comparable with those of this case.

Figure 19 shows the effect of the 2.74 N-m torque applied about the spacecraft y_S-axis with the fine pointing control law deactivated to show the coarse pointing control response. The conditions of the previous case are used. The theoretical pointing error caused by this torque with only the coarse pointing control law is 0.9 arc second. The simulation verifies this value and the desired damping of 0.7. Reaction-wheel time histories are not shown since there is no reaction-wheel response for this case. The outer gimbal responses are similar to the previous case as is expected. The 2.74 N-m torque was applied about the spacecraft z_S-axis with no fine pointing and the results were similar to the results of this case.

Effect of initial pointing errors.- Figure 20 shows the response of the spacecraft to a 10-arc-second initial roll position error. The gimbal angles are in the reference positions initially and each energy-wheel spin rate is at 25 000 rpm. The pitch and yaw pointing errors and the inner gimbal angles are also shown in the figure. The time scale is 1 second per division. The roll response is close to the desired response having a natural frequency of 0.229 Hz and a damping ratio of 0.7. There does not appear to be any cross coupling to the pitch or yaw axes. The inner gimbal motion required to null the error is very small as expected.

Figure 21 shows the response of the spacecraft to a 1-arc-second initial pitch axis pointing error. The system conditions are the same as in the previous case. Here the reaction-wheel speed responses are shown together with the responses for the outer gimbals 2 and 3. The reaction wheels null the pointing error and the outer gimbals null the reaction-wheel speeds so that after approximately 5 seconds, the system is in steady state with the initial error nulled. Torque limiting at 4 N-m occurs as noted by the initial straight-line segments in the figure. A similar case was simulated for the z_S-axis and the results were comparable.

Effect of gravity-gradient disturbance torques.- Figure 22 shows the results of the simulation of the RAM-TAG system in the baseline orbit. The spacecraft orientation is solar inertial with the roll axis out of the orbit plane at an angle of 45°. This is a worst case in the sense that the bias gravity-gradient torque is maximum in this orientation. Initially, the inner and outer gimbals are in their reference orientations, the energy-wheel speeds are at 25 000 rpm and charge torques of 0.45 N-m per wheel are applied to them. The reaction wheels are at zero speed and there are no initial spacecraft pointing errors. The time scale is 5 minutes per division.

Figure 22(a) shows the spacecraft pointing errors during the simulation. The apparent spikes on the x_S-axis time history are roll-angle errors that occurred every 5 seconds caused by the 460-msec period of control computation during which the roll axis is uncontrolled. The magnitude of these errors is far below the allowable maximum of ±5 arc seconds. The pitch and yaw pointing errors follow the gravity torques as expected and the maximum pointing errors are 0.005 arc second and 0.0035 arc second, respectively.

Figure 22(b) shows the outer gimbal angle time histories. These data were sampled every 5 minutes because of the lack of additional strip chart recorders. The sampling frequency was adequate because of the relatively slow gimbal motion. It is noted that outer gimbal 1 remains relatively close to its reference position whereas gimbals 2 and 3 move away from their reference positions. This motion is caused by the bias gravity-gradient torque. The magnetic torquer, which is not included in this simulation, would minimize this motion. It is pointed out that the system, as sized here, has more angular momentum than is required for control only. Including the energy storage feature in the attitude control system generally will result in a control system with excess angular momentum. In a conventional CMG system the gravity-gradient bias torque could cause saturation in one orbit, whereas only 40° of gimbal travel occurs here.

Figure 22(c) shows the inner gimbal time histories. Note that the vertical scale is different from the outer gimbal time histories. Theoretically, there should be no inner gimbal motion. It is felt that this motion was due to computational inaccuracies. Finally, the bottom curve in figure 22(c) is representative of the three energy-wheel speed variations during the orbit. Small changes due to the peak power loads do not show up in these data but the peak loads were simulated. No discernible pointing errors due to these loads were observed.

Effect of a reorientation rate acquisition command.- Figure 23 shows the results of the simulation of a spacecraft reorientation rate acquisition. There are no external torques acting on the vehicle. The TAG energy wheels are at 25 000 rpm, and the gimbals are initially in their reference positions. Shown in the figure are spacecraft pitch angle θ, pitch rate q, and the three outer gimbal angles. The time scale is 1 minute per division. A pitch rate of $6^{\circ}/\text{min}$ is commanded at $t = 0$, and it is acquired in approximately 4 minutes. The initial angular acceleration of the spacecraft is approximately $6^{\circ}/\text{min}^2$, the desired value. The initial outer gimbal rates for units two and three are approximately $0.31^{\circ}/\text{sec}$ which is the theoretical value based on the angular momentum magnitudes, gimbal angles, and desired torque. Gimbals 2 and 3 reach steady-state angles of approximately 142° and -141°, respectively, as determined from the figure. These angles give a total calculated angular momentum of

$$\underline{RH} \doteq \begin{Bmatrix} 0 \\ -711 \\ 0 \end{Bmatrix} \text{ N-m-sec}$$

The angular momentum of the spacecraft based on the angular rate of 6^{o}/min is calculated to be

$$\underline{H_S} = \begin{Bmatrix} 0 \\ 709 \\ 0 \end{Bmatrix} \text{ N-m-sec}$$

Theoretically, $\underline{RH}$ should equal $-\underline{H_S}$ in this case; inaccuracy in reading the final gimbal angles is thought to be the cause of the difference.

A yaw-rate acquisition was considered and the simulated motion checked closely with predicted motion.

In these cases additional computation equipment was not available to simulate the spacecraft rate vector – TAG system momentum vector cross-product term $[\underline{\Omega}]\underline{RH}$ that appears in equation (10). In these cases this term would have been equal to zero anyway because $\underline{\Omega}$ and $\underline{RH}$ were colinear throughout the maneuvers.

CONCLUDING REMARKS

A conceptual design for a double-gimbal reaction-wheel—energy-wheel device, which has three-axis attitude control torque and electrical energy storage capability, is given. A mathematical model for the three-axis gyroscope (TAG) is developed, and a system comprised of multiple TAG units with a digital flight computer is proposed for the attitude control and energy storage system of a spacecraft. Algorithms that determine torques required for spacecraft fine pointing, coarse pointing, and reorientation are formulated. TAG gimbal rate laws, reaction-wheel torque laws, and energy-wheel torque laws are derived that produce the required control torques while minimizing functions of TAG gimbal angles, gimbal rates, reaction-wheel speeds, and energy-wheel speed differences. A magnetic torquer is proposed for TAG system desaturation, and a control law is derived that minimizes a function of the magnetic energy required while providing a net dump of angular momentum each orbit.

To evaluate the design concept, a three-TAG system is sized for a proposed shuttle-launched research and applications module (RAM); and a computer simulation of the TAG system and spacecraft dynamics is developed and used. Various modes of

operation, including spacecraft fine pointing in the presence of time-varying gravity-gradient disturbance torques, are considered. Time-history plots of critical variables are presented and discussed for the cases studied.

The results of the analysis and simulation indicate the following:

1. Combined three-axis attitude control and electrical energy storage using the TAG concept is theoretically feasible.

2. In the derivation of the TAG gimbal rate control law, minimizing functions of gimbal angles and rates causes the gimbals to favor continuously their reference orientation and thereby eliminate the gimbal drift anomaly that often leads to attitude control system instabilities.

3. Including reaction-wheel speeds in the gimbal rate control law and the reaction-wheel control law provides continuous automatic reaction-wheel desaturation without causing any net torque to be applied to the spacecraft.

4. The digital gimbal rate control law which is based on minimization of functions of the reaction-wheel speeds, gimbal angles, and gimbal rates with constrained output torque requirements gives perfect command torque – output torque matching, maintains the gimbals near their reference orientation, and continuously desaturates the reaction wheels. A gain matrix update frequency of once every 5 seconds and a gimbal rate command update frequency of once every 80 msec are adequate.

5. Typically, the energy storage requirements cause the angular momentum level of the TAG units to be higher than necessary for control only (by a factor of three at maximum wheel speed for the example). This condition has the advantage of giving the control system more gravity-gradient bias torque capability and maneuver rate capability but has the disadvantage of requiring more precise gimbal rate control.

6. For the example mission studied, the pointing errors caused by gravity-gradient torques are controlled below the required level of 0.017 arc second. Uncontrolled pointing errors reach estimated maximum values of 330 arc seconds in one orbit.

7. Fabrication and testing of a laboratory prototype would be required for complete determination of the feasibility of the TAG concept.

8. Hardware anomalies such as gimbal torque motor hysteresis break-out torque, gimbal tachometer and resolver resolution, spacecraft attitude sensor deadbands, reaction-wheel tachometer resolution, and signal noise throughout the control system will limit the ultimate pointing capability of the TAG system. Final hardware design studies should consider these nonlinearities.

9. Control system stability was not considered in this study since the actuators and sensors were considered as perfect. Final design studies including actuator and

sensor dynamics should consider control system stability because of the high loop gains required for fine pointing.

Langley Research Center,
National Aeronautics and Space Administration,
Hampton, Va., March 1, 1974.

APPENDIX A

TORQUE EQUATION FOR THE TAG UNIT

It is assumed that the TAG unit, shown schematically in figures 1, 2, and 3, may be represented analytically by a combination of four rigid components: the two axisymmetric wheels, the inner gimbal, and the outer gimbal. A rotating spacecraft axis system is used as reference for the TAG elements. It is also assumed that for each component, geometric axes are principal axes, and the wheels' spin axis is coincident with the inner gimbal y_I-axis as shown in figure 3.

The torque acting on a spacecraft due to forced angular motion of the TAG components is equal to the negative of the time derivative of the TAG unit angular momentum. The TAG momentum is found by computing the momentum of the four components separately, transforming each to the spacecraft axes, and then adding them to get the total.

The angular momentum of the outer gimbal taken separately is given in outer gimbal coordinates by

$$\underline{H}_O^O = I_O\left(\underline{\omega}_O^O + T_{O/S}^T\underline{\Omega}\right) \tag{A1}$$

where the outer gimbal inertia matrix is given by

$$I_O = \text{diag}\begin{pmatrix} I_{Ox} & I_{Oy} & I_{Oz} \end{pmatrix}$$

The outer gimbal angular velocity, relative to the spacecraft, is given in terms of the relative outer gimbal rate $\dot{\alpha}$ as

$$\underline{\omega}_O^O = \begin{bmatrix} \dot{\alpha} & 0 & 0 \end{bmatrix}^T$$

The matrix $T_{O/S}^T$ is the inverse of the outer gimbal to spacecraft axes orthogonal transformation, and is given as

$$T_{O/S}^T = \begin{bmatrix} 1 & 0 & 0 \\ 0 & c\alpha & s\alpha \\ 0 & -s\alpha & c\alpha \end{bmatrix}$$

The spacecraft angular velocity $\underline{\Omega}$ is given in terms of the body rates as

$$\underline{\Omega} = \begin{bmatrix} p & q & r \end{bmatrix}^T$$

The outer gimbal angular momentum given by equation (A1) may be expressed in spacecraft coordinates by using the transformation $T_{O/S}$ as

$$\underline{H}_O^S = T_{O/S}\underline{H}_O^O = T_{O/S}I_O\underline{\omega}_O^O + T_{O/S}I_O T_{O/S}^T\underline{\Omega} \tag{A2}$$

The angular momentum of the inner gimbal, taken separately, is given in inner gimbal coordinates by

$$\underline{H}_I^I = I_I\left(\underline{\omega}_I^I + T_{I/S}^T\underline{\Omega}\right) \tag{A3}$$

where the inner gimbal inertia matrix is given by

$$I_I = \text{diag}\begin{pmatrix} I_{Ix} & I_{Iy} & I_{Iz}\end{pmatrix}$$

The angular velocity of the inner gimbal with respect to the spacecraft is given in terms of the relative gimbal rates $\dot{\alpha}$ and $\dot{\beta}$ as

$$\underline{\omega}_I^I = \begin{bmatrix}\dot{\alpha}c\beta & -\dot{\alpha}s\beta & \dot{\beta}\end{bmatrix}^T$$

The matrix $T_{I/S}^T$ is the inverse of the inner gimbal to spacecraft axes orthogonal transformation, and is given as

$$T_{I/S}^T = \begin{bmatrix} c\beta & c\alpha s\beta & s\alpha s\beta \\ -s\beta & c\alpha c\beta & s\alpha c\beta \\ 0 & -s\alpha & c\alpha \end{bmatrix}$$

The inner gimbal angular momentum given by equation (A3) may be expressed in spacecraft coordinates by using the transformation $T_{I/S}$ as

$$\underline{H}_I^S = T_{I/S}\underline{H}_I^I = T_{I/S}I_I\omega_I^I + T_{I/S}I_I T_{I/S}^T\underline{\Omega} \tag{A4}$$

The angular momentum of the two wheels is given in inner gimbal coordinates by

$$\underline{H}_W^I = I_L\left(\underline{\omega}_L^I + \underline{\omega}_I^I + T_{I/S}^T\underline{\Omega}\right) + I_H\left(\underline{\omega}_H^I + \underline{\omega}_I^I + T_{I/S}^T\underline{\Omega}\right) \tag{A5}$$

where the first group of terms represents the angular momentum of the reaction wheel, and the second group represents the momentum of the energy wheel. The inertia matrix for the reaction wheel is given by

$$I_L = \text{diag}\begin{pmatrix} I_{LT} & I_{LA} & I_{LT} \end{pmatrix}$$

and the angular velocity of the reaction wheel with respect to the inner gimbal is given by

$$\underline{\omega}_L^I = \begin{bmatrix} 0 & \omega_L & 0 \end{bmatrix}^T$$

The inertia matrix for the energy wheel is given by

$$I_H = \text{diag}\begin{pmatrix} I_{HT} & I_{HA} & I_{HT} \end{pmatrix}$$

and the angular velocity of the energy wheel with respect to the inner gimbal is given by

$$\underline{\omega}_H^I = \begin{bmatrix} 0 & \omega_H & 0 \end{bmatrix}^T$$

The other terms in equation (A5) have been defined previously. The angular momentum of the two wheels given by equation (A5) may be expressed in spacecraft coordinates by using the transformation $T_{I/S}$ as

$$\underline{H}_W^S = T_{I/S}\underline{H}_W^I = T_{I/S}I_L\left(\underline{\omega}_L^I + \underline{\omega}_I^I + T_{I/S}^T\underline{\Omega}\right) + T_{I/S}I_H\left(\underline{\omega}_H^I + \underline{\omega}_I^I + T_{I/S}^T\underline{\Omega}\right) \quad \text{(A6)}$$

The total angular momentum of the TAG unit, expressed in spacecraft coordinates, is found by combining equations (A2), (A4), and (A6) as

$$\begin{aligned} \underline{H}_T^S &= \underline{H}_O^S + \underline{H}_I^S + \underline{H}_W^S \\ &= T_{O/S}I_O\underline{\omega}_O^O + T_{O/S}I_OT_{O/S}^T\underline{\Omega} + T_{I/S}I_I\underline{\omega}_I^I + T_{I/S}I_IT_{I/S}^T\underline{\Omega} \\ &\quad + T_{I/S}I_L\left(\underline{\omega}_L^I + \underline{\omega}_I^I + T_{I/S}^T\underline{\Omega}\right) + T_{I/S}I_H\left(\underline{\omega}_H^I + \underline{\omega}_I^I + T_{I/S}^T\underline{\Omega}\right) \end{aligned} \quad \text{(A7)}$$

The output torque equation for the TAG unit is obtained by taking the negative time derivative of $\underline{H}_T^S$ in the moving spacecraft coordinate system as

$$\underline{T}_U = -\frac{d\underline{H}_T^S}{dt} = -\dot{\underline{H}}_T^S - \left[\underline{\Omega}\right]\underline{H}_T^S \quad \text{(A8)}$$

where the vector $\underline{T}_U$ represents the torque on the spacecraft. The first term on the right-hand side represents the rate of change of TAG angular momentum with respect to the spacecraft, and the second term represents the rate of change of TAG angular momentum due to the angular velocity of the spacecraft. The first term of equation (A8) involves

the time derivatives of products of the transformation matrices, the gimbal and wheel angular velocities, and the spacecraft angular velocity. The second term in equation (A8) represents the vector cross product of the spacecraft angular velocity with the TAG angular momentum.

APPENDIX B

RAM-TAG SYSTEM CONSTANTS

In this appendix the constants in the three TAG system control laws are derived for the example RAM spacecraft and mission. These parameters are used in the simulation described in appendix C.

The elements of the coarse pointing and fine pointing attitude gain matrices K_{AC} and K_{AF} used in equations (5) and (6) are determined by dividing an assumed maximum disturbance torque per axis by the pointing stability requirement. The disturbance torque for y_S- and z_S-axis is taken as the maximum gravity-gradient torque plus the maximum power generation torque. For the x_S-axis, only the power torque is used.

The gravity-gradient torque is computed from equations (D7), (D8), and (D9) of appendix D. For the example spacecraft $T_{Dx} = 0$ and the maximum torque along the y_S- and z_S-axis is given as

$$T_{D,max} = \frac{3}{2}\omega_O^2\left(I_T - I_x\right)$$

With $\omega_O = \frac{2\pi}{90}$ rad/min, $I_T = 406\ 000$ kg-m^2, and $I_x = 40\ 600$ kg-m^2,

$$T_{D,max} = 0.74 \text{ N-m}$$

The maximum power generation torque applied to the spacecraft occurs with the three TAG momentum vectors alined at the minimum allowable wheel speed and at the maximum power output. The minimum wheel speed for the example system is 22 500 rpm and the maximum generator power is 4820 W. This vector alinement condition is not used because the attitude control system cannot function in this orientation. An arbitrary condition is selected where each TAG momentum vector is approximately 13° away from, and equally spaced around, the total momentum vector. These conditions give a power torque of approximately 2.0 N-m.

The y_S- and z_S-axis torque for the attitude gain calculation is taken as 2.74 N-m, and for the x_S-axis, 2.0 N-m. From table I, the y_S- and z_S-axis fine pointing stability level is ± 0.017 arc second or 8.24×10^{-8} rad. Dividing this value into the y_S, z_S torque of 2.74 N-m gives the fine pointing attitude gains as

$$K_{AFy} = -3.32 \times 10^7 \text{ N-m/rad}$$

$$K_{AFz} = -3.32 \times 10^7 \text{ N-m/rad}$$

where the minus sign is required to give a stable system. The y_S- and z_S-axis coarse pointing stability requirement is ±0.5 arc second or 2.43×10^{-6} rad. Dividing the y_S, z_S torque of 2.74 N-m by 2.43×10^{-6} rad gives

$$K_{ACy} = -1.13 \times 10^{6} \text{ N-m/rad}$$

$$K_{ACz} = -1.13 \times 10^{6} \text{ N-m/rad}$$

The x_S-axis coarse pointing stability requirements is ±5 arc seconds or 2.43×10^{-5} rad. Dividing the x_S-axis torque of 2.0 N-m by 2.43×10^{-5} rad gives

$$K_{ACx} = -8.23 \times 10^{4} \text{ N-m/rad}$$

The fine and coarse pointing angular rate gains are calculated to give the controlled motion a theoretical second-order damping of 0.7. Recalling the formula for the rate gain in terms of damping ratio ρ, moment of inertia I_T, and attitude gain K_A gives

$$K_R = -2\rho\sqrt{-K_A I_T}$$

The fine pointing rate gains for the y_S- and z_S-axis are computed with $I_T = 4.06 \times 10^{5}$ kg-m^2 as

$$K_{RFy} = -5.14 \times 10^{6} \text{ N-m/(rad/sec)}$$

$$K_{RFz} = -5.14 \times 10^{6} \text{ N-m/(rad/sec)}$$

The coarse pointing rate gain for the x_S-axis is computed with $I_x = 4.06 \times 10^{4}$ kg-m^2 as

$$K_{RCx} = -8.09 \times 10^{4} \text{ N-m/(rad/sec)}$$

The coarse pointing rate gains for the y_S- and z_S-axis are computed as

$$K_{RCy} = -9.48 \times 10^{5} \text{ N-m/(rad/sec)}$$

$$K_{RCz} = -9.48 \times 10^{5} \text{ N/m/(rad/sec)}$$

The TAG reaction-wheel desaturation gain K_R in equation (26) is taken so that the 2.74 N-m disturbance torque causes the maximum reaction-wheel speed, given previously as 85 rpm. The gain is computed by dividing the disturbance torque by the wheel speed to get

$K_R = 0.308$ N-m/(rad/sec)

The energy-wheel parameter k given in equation (32) is arbitrarily selected to give an energy equalization time constant of 6 minutes. The parameter k is thus taken to be $k = 360$ seconds. The value of k is not critical and should be adjusted to give the best responses in practice.

The constants F_A and F_B in the gimbal angle function $f(\underline{\gamma})$ given by equations (18) and (19) are taken to give 1^o/sec gimbal rate commands for outer gimbal angles of 90^o and for inner gimbal angles of 45^o. This requirement gives

$F_A = 0.0111$ (rad/sec)/rad

$F_B = 0.0222$ (rad/sec)/rad

APPENDIX C

RAM-TAG SIMULATION DESCRIPTION

Simulated Systems

In this appendix a computer simulation for the RAM-TAG system is described. The simulated systems considered are the RAM spacecraft dynamics and TAG attitude control and power storage system functions during observational periods. The simulation is based on the following simplifying assumptions:

(1) The spacecraft and all TAG system structural components are rigid bodies and the TAG gimbals are assumed to be weightless.

(2) During fine pointing, small-angle approximations are used to describe the spacecraft motion, and the spacecraft angular rates are low enough to neglect the term $[\underline{\Omega}]\underline{RH}$ in the TAG torque equation.

(3) Gravity-gradient and power-transfer torques are the only disturbances applied to the spacecraft.

(4) TAG gimbal drive servos are ideal in that actual gimbal rates are equal to commanded rates.

(5) Spacecraft angular rate and position sensors are approximated by constant gains.

Simulation System

The simulation system is comprised of Electronic Associates, Inc. (EAI) 680 analog computer, an EAI 640 digital computer, an EAI 693 interface system, and various display equipment. The analog computer is used to simulate both the spacecraft dynamics and the TAG system dynamics and to carry out certain algebraic calculations. The digital computer is used to simulate the attitude control and power storage functions of the spacecraft flight computer and to perform additional calculations associated with the simulation. An overall block diagram of the simulation is given in figure 9. The equations in this diagram and the division of computational tasks are discussed.

Analog Computations

The simulation block diagram given in figure 9 shows the equations that are implemented on the analog computer. All computations are done in real time. Time is generated explicitly by integrating a constant so that 10 000 seconds of simulation is possible.

The spacecraft equations of motion take on a particularly simple form for simulation of the fine pointing mode. These equations are given by

$$\dot{\underline{\Omega}} = I_S^{-1}\left(\underline{T}_R + \underline{T}_P + \underline{T}_D\right) \tag{C1}$$

where $\dot{\underline{\Omega}}$ is the spacecraft total angular acceleration vector defined in terms of body-axis components as

$$\dot{\underline{\Omega}} = \begin{bmatrix}\dot{p} & \dot{q} & \dot{r}\end{bmatrix}^T$$

The mass moment of inertia matrix I_S is given by equation (36). The three torques $\underline{T}_R$, $\underline{T}_P$, and $\underline{T}_D$ are the TAG rotor acceleration reaction torque, the TAG precession reaction torque, and the external disturbance torque, respectively. The TAG rotor acceleration reaction torque is computed by adding equations (26) and (32) to give

$$\underline{T}_R = -R\left(\underline{T}_L + \underline{T}_H\right) \tag{C2}$$

The TAG precession reaction torque $\underline{T}_P$ is computed according to equation (14) by neglecting the $[\underline{\Omega}]R\underline{H}$ term. The external disturbance torque $\underline{T}_D$ is computed by the digital computer and is covered later.

The spacecraft body rates are computed by integrating equation (C1). The spacecraft angular displacements are determined by integrating the body rates.

The energy-wheel and reaction-wheel spin rate equations of motion have the following form:

$$\dot{\underline{\omega}}_H = \frac{1}{I_{HA}}\underline{T}_H \tag{C3}$$

$$\dot{\underline{\omega}}_L = \frac{1}{I_{LA}}\underline{T}_L \tag{C4}$$

The rotor torques $\underline{T}_H$ and $\underline{T}_L$ are computed according to equations (32) and (26) where the total energy E_T is computed by using equation (30) and the average angular momentum per TAG unit H is computed by using equation (13). The rotor rates are computed by integrating equations (C3) and (C4).

The TAG gimbal angles are computed by integrating the command gimbal rates computed digitally from equation (20). Trigonometric function generators are used to compute the sine and cosine of each gimbal angle.

The spacecraft coarse pointing and fine pointing command control torques are computed by using equations (5) and (6). Limiters are used in the fine pointing torque calculations to limit the command torque to 4 N-m (the baseline RAM reaction-wheel torque limits).

The spacecraft electrical power profile is calculated according to the relation given by

$$P_T = P_D + P_C(t) + P_{DP}(t)$$

where $P_D = -3400$ W and $P_C(t)$ is either zero or 6900 W when the spacecraft is in sunlight. The term $P_{DP}(t)$ is zero normally and -450 W during peak power loads.

Digital Calculations

The simulation block diagram given in figure 9 summarizes the calculations that are implemented on the digital computer. Time critical calculations are updated as quickly as possible; in the present case, about every 80 msec. Non-time-critical calculations are performed periodically by interrupting the fast loop every 5 seconds. These calculations take approximately 460 msec. The 5-second period was not critical and could be shortened to 1 second or lengthened to 10 seconds without affecting the simulation results.

Figure 9 shows the calculations that are repeated every 5 seconds. The gravity-gradient disturbance torque vector $\underline{T}_D$, derived in appendix D and given by equations (D7), (D8), and (D9), is computed by the digital computer. Time t generated by the analog computer is input to these equations. The constants required include the spacecraft pitch, yaw, and roll moments of inertia. The orbit frequency ω_O is taken as 1 cycle per 90 minutes. The initial Euler angles θ and ψ are defined in figure 10 and are constants for each simulation run.

Several coefficient and transformation matrices are updated every 5 seconds. The elements of the matrix R given by equation (12) with $n = 3$ are computed in terms of the sines and cosines of the gimbal angles computed by the analog computer. The matrix $\tilde{R}$ (the truncated version of R), given by equation (23), is used to form the matrix $G \triangleq \tilde{R}^T\left(\tilde{R}\tilde{R}^T\right)^{-1}$ in equation (26). The inverse of $\tilde{R}\tilde{R}^T$ is determined analytically so that

$$\tilde{R}^T\left(\tilde{R}\tilde{R}^T\right)^{-1} = \frac{1}{D}\begin{bmatrix} c\alpha_1 c\beta_1 RR_{22} - s\alpha_1 c\beta_1 RR_{12} & s\alpha_1 c\beta_1 RR_{11} - c\alpha_1 c\beta_1 RR_{12} \\ c\alpha_2 c\beta_2 RR_{22} - s\alpha_2 c\beta_2 RR_{12} & s\alpha_2 c\beta_2 RR_{11} - c\alpha_2 c\beta_2 RR_{12} \\ c\alpha_3 c\beta_3 RR_{22} - s\alpha_3 c\beta_3 RR_{12} & s\alpha_3 c\beta_3 RR_{11} - c\alpha_3 c\beta_3 RR_{12} \end{bmatrix} \quad \text{(C5)}$$

where

$$RR_{11} = \sum_{1}^{3} c^2\alpha_i c^2\beta_i$$

$$RR_{12} = \sum_{1}^{3} c\alpha_i s\alpha_i c^2\beta_i$$

$$RR_{22} = \sum_{1}^{3} s^2\alpha_i c^2\beta_i$$

and the determinant of $\tilde{R}\tilde{R}^T$ is given by

$$D = RR_{11}RR_{22} - RR_{12}^2$$

The elements of the 3 by 6 matrix Γ are computed according to equation (11) with $n = 3$. The matrix $C \triangleq Q^{-1}\Gamma^T\left(\Gamma Q^{-1}\Gamma^T\right)^{-1}$ in equation (20) (with $Q = I$) is computed, where the inverse of $\Gamma\Gamma^T$ is calculated by using a standard matrix algebra subroutine. The vector $\underline{f}(\gamma)$ given by equations (18) and (19) with $n = 3$ is computed in terms of the sines and cosines of the gimbal angles with $F_A = 0.0111$ (rad/sec)/rad, $F_B = 0.0222$ (rad/sec)/rad, $\alpha_{10} = 0^o$, $\alpha_{20} = 120^o$, and $\alpha_{30} = -120^o$.

The time-critical digital calculations involve the gimbal rate commands. The TAG gimbal rate control law given by equation (20) is updated at a rate of about once every 80 msec, and the desired gimbal rate torque $\underline{T}_G$ is given by equation (16) with $m = 0$ for the fine pointing simulation. The computation of the new $\dot{\underline{\gamma}}_D$ involves the coefficient matrices R, C, and Γ as well as the vector $\underline{f}$ and analog variables H, $\underline{T}_{CD}$, $\underline{\omega}_L$, and $\underline{T}_H$.

Interface Operations

The hybrid computer interface system transfers data from the analog computer to the digital computer and transfers (and operates on) data from the digital computer to the analog computer. Figure 9 summarizes the interface operations performed.

Twenty-three channels of analog data are converted to digital words every cycle through the computation loop. This conversion means that the variables $\underline{T}_H$, t, H, $\underline{\omega}_L$, $\underline{T}_{CD}$, and the sines and cosines of the gimbal angles are updated in the digital computer approximately every 80 msec.

Six digital to analog multipliers (DAMs) transfer new values of $\dot{\underline{\gamma}}_D$ to the analog computer at the 80 msec rate. Three DAMs update $\underline{T}_D$ every cycle. Six DAMs update G every cycle and multiply the fine pointing command $\underline{T}_{FD}$ continuously. Nine DAMs update -R every cycle and form the product $R\left(\underline{T}_L + \underline{T}_H\right)$ continuously. Fifteen digitally controlled attenuators (DCAs) update Γ every cycle and form the product $\Gamma^T\dot{\underline{\gamma}}_D$ continuously.

APPENDIX D

SPACECRAFT GRAVITY-GRADIENT TORQUE EQUATION

This appendix formulates the gravity-gradient torque acting on an axisymmetric spacecraft in a circular orbit about a spherical planet in terms of time and inertial Euler angles. This formulation was needed for spacecraft control system simulation and was not found in the literature.

The gravitational torque acting on a spacecraft in circular orbit about a planet is given in reference 16 as

$$\underline{T}_D = 3\omega_O^2\left(\hat{r} \times I_S\hat{r}\right) \tag{D1}$$

where ω_O is the mean orbital angular velocity, $\hat{r}$ is a unit vector in the direction of the line joining the mass center of the planet and the spacecraft, and I_S is the inertia matrix for the spacecraft. The method used to express $\underline{T}_D$ about body axes is to determine $\hat{r}$ in body coordinates and then expand equation (D1) in terms of $\hat{r}$ and I_S. Figure 10 shows the coordinate systems used. An inertial axis system $\left(X_I,Y_I,Z_I\right)$ is assumed such that the origin is at the mass center of the attracting planet. The X_I-axis passes through the point of perigee and the Y_I-axis lies in the orbit plane in such a position that the Z_I-axis is normal to the orbit plane in the direction of the orbit angular momentum vector. An orbit axis system $\left(X_O,Y_O,Z_O\right)$ is assumed so that its origin moves with the spacecraft center of mass with the X_O-axis in the direction of the line from the origin of the $\left(X_I,Y_I,Z_I\right)$ system to the origin of the $\left(X_O,Y_O,Z_O\right)$ system. The Z_O-axis is parallel to the Z_I-axis, and the Y_O-axis completes the right-handed set. At time equal to zero the $\left(X_O,Y_O,Z_O\right)$ system is alined with the $\left(X_I,Y_I,Z_I\right)$ system. The angle between the Z_O-axis and the X_I-axis is $\omega_O t$. The spacecraft body-axis system $\left(x_S,y_S,z_S\right)$ has its origin at the spacecraft center of mass and is related to the inertial axis system by the conventional Euler angles as shown in figure 10. The unit vector $\hat{r}$ in orbit coordinates has the following form:

$$\hat{r}^O = \begin{bmatrix}1 & 0 & 0\end{bmatrix}^T \tag{D2}$$

This vector is expressed in inertial coordinates by the following transformation:

$$\hat{r}^R = \begin{bmatrix} c\omega_O t & -s\omega_O t & 0 \\ s\omega_O t & c\omega_O t & 0 \\ 0 & 0 & 1 \end{bmatrix} \begin{Bmatrix} 1 \\ 0 \\ 0 \end{Bmatrix} = \begin{Bmatrix} c\omega_O t \\ s\omega_O t \\ 0 \end{Bmatrix} \tag{D3}$$

The inertial axes to spacecraft body-axis transformation is given by

$$T_{I/B} = \begin{bmatrix} c\psi c\theta & s\psi c\theta & -s\theta \\ -s\psi c\phi + c\psi s\theta\, s\phi & c\psi c\phi + s\psi s\theta\, s\phi & c\theta\, s\phi \\ s\psi s\phi + c\psi s\theta\, c\phi & s\psi s\theta\, c\phi - c\psi s\phi & c\theta\, c\phi \end{bmatrix} \tag{D4}$$

Then the unit vector $\hat{r}$ may be expressed in the body-axis system as

$$\hat{r}^S = T_{I/B}\hat{r}^R = \begin{Bmatrix} r_{xS} \\ r_{yS} \\ r_{zS} \end{Bmatrix} = \begin{Bmatrix} c\omega_O t c\psi c\theta + s\omega_O t s\psi c\theta \\ c\omega_O t\left(c\psi s\theta s\phi - s\psi c\phi\right) + s\omega_O t\left(c\psi c\phi + s\psi s\theta s\phi\right) \\ c\omega_O t\left(s\psi s\phi + c\psi s\theta c\phi\right) + s\omega_O t\left(s\psi s\theta c\phi - c\psi s\phi\right) \end{Bmatrix} \tag{D5}$$

The gravity-gradient torques about the principal spacecraft body axes may now be calculated by using equations (D1) and (D5) as

$$\underline{T}_D = 3\omega_O^2 \begin{Bmatrix} r_{yS} r_{zS}\left(I_z - I_y\right) \\ r_{xS} r_{zS}\left(I_x - I_z\right) \\ r_{xS} r_{yS}\left(I_y - I_x\right) \end{Bmatrix} \tag{D6}$$

For the present study it is assumed that the spacecraft is axisymmetric so that $I_y = I_z = I_T$. Making these substitutions into equation (D6) shows that there is no gravity torque about the axis of symmetry; that is,

$$T_{Dx} = 0 \tag{D7}$$

It is also assumed for computational convenience that the roll angle ϕ of the spacecraft is maintained near zero so that $\cos\phi \approx 1$ and $\sin\phi \approx 0$. Making these substitutions into equation (D6), using equation (D5), and $I_y = I_z = I_T$ gives

$$T_{Dy} = -\frac{3}{2}\omega_O^2\left(I_T - I_x\right)\left(s2\theta + s2\theta c2\left(\omega_O t - \psi\right)\right) \tag{D8}$$

$$T_{Dz} = \frac{3}{2}\omega_O^2\left(I_T - I_x\right)c\theta\, s2\left(\omega_O t - \psi\right) \tag{D9}$$

Equations (D7), (D8), and (D9) may be used in a real-time simulation to provide a reasonable approximation to the gravity-gradient torques acting on an axisymmetric spacecraft in a circular orbit about a spherical planet.

REFERENCES

1. Lyons, M. G.; Lebsock, K. L.; and Scott, E. D.: Double Gimballed Reaction Wheel Attitude Control System for High Altitude Communications Satellites. AIAA Paper No. 71-949, Aug. 1971.

2. Mork, H. L.: Synthesis and Design of a Gimbaled Reaction Wheel Attitude Stabilization Package (GRASP). AIAA Paper No. 71-950, Aug. 1971.

3. Auclair, Gary F.: Advanced Reaction Wheel Controller for Spacecraft Attitude Control. AIAA Paper No. 69-855, Aug. 1969.

4. Kurzhals, Peter R.; and Grantham, Carolyn: A System for Inertial Experiment Pointing and Attitude Control. NASA TR R-247, 1966.

5. Kennedy, H. B.: A Gyro Momentum Exchange Device for Space Vehicle Attitude Control. AIAA J., vol. 1, no. 5, May 1963, pp. 1110-1118.

6. Schindelin, Jürgen·W.: Space Vehicle Attitude Stabilization and Control by a Three-Degree of Freedom Control Moment Gyro With Controllable Gyro Spin Velocity. Z. Flugwiss., vol. 17, no. 4, 1969, pp. 131-134.

7. Kranton, Jack: Application of Optimal Control Theory to Attitude Control With Control Moment Gyroscopes (CMGs). Ph. D. Diss., George Washington Univ., Feb. 1970.

8. Hart, L. R.; et al.: Application of Magnetic Torquing for Desaturation of Control Moment Gyros in Space Vehicle Control. AFFDL-TR-67-8, U.S. Air Force, June 1967. (Available from DDC as AD 817 503.)

9. Lawson, Louis J.: Design and Testing of High Energy Density Flywheels for Application to Flywheel/Heat Engine Hybrid Vehicle Drives. 1971 Intersociety Energy Conversion Engineering Conference, Soc. Automat. Eng., Inc., c.1971, pp. 1142-1150.

10. Rabenhorst, David W.: Potential Applications for the Superflywheel. Paper presented at 1971 Intersociety Energy Conversion Engineering Conference (Boston, Mass.), Aug. 1971.

11. Notti, J. E.; Cormack, A., III; and Schmill, W. C.: Integrated Power/Attitude Control System (IPACS) Study. Vol. 1 – Feasibility Studies. NASA CR-2383, 1974.

12. Notti, J. E.; Cormack, A., III; Schmill, W. C.; and Klein, W. J.: Integrated Power/Attitude Control System (IPACS) Study. Vol. 2 – Conceptual Designs. NASA CR-2384, 1974.

13. Anderson, Willard W.; and Keckler, Claude R.: An Integrated Power/Attitude Control System (IPACS) for Space Vehicle Application. Paper Presented at Fifth IFAC Symposium on Automatic Control in Space (Genoa, Italy), June 1973.

14. Grubin, Carl: Two Impulse Attitude Reorientation of an Asymmetric Spinning Vehicle. AIAA Symposium on Structural Dynamics and Aeroelasticity, Aug.-Sept., 1965, pp. 245-249.

15. Gelfand, I. M.; and Fomin, S. V. (Richard A. Silverman, transl.): Calculas of Variations. Prentice-Hall, Inc., c.1963.

16. Anon.: Spacecraft Gravitational Torques. NASA SP-8024, 1970.

TABLE I.- EXAMPLE A303B RAM EXPERIMENT SUPPORT REQUIREMENTS

Pointing:	
Orientation	Solar
Accuracy:	
Acquisition (no support from experiment)	±30 arc sec
Experiment pointing (supported by experiment-supplied aspect error):	
Pitch and yaw	±1 arc sec
Roll	±5 arc sec
Stability (supported by experiment-supplied aspect error):	
Pitch and yaw	±0.5 arc sec (basic), ±0.017 arc sec fine pointing
Roll	±5 arc sec
Observation time	0.75 hr
Slew rate, acceleration	6^{o}/min, 6^{o}/min^2
Orbit:	
Altitude	279 km
Inclination	55^{o}
Period	90 min

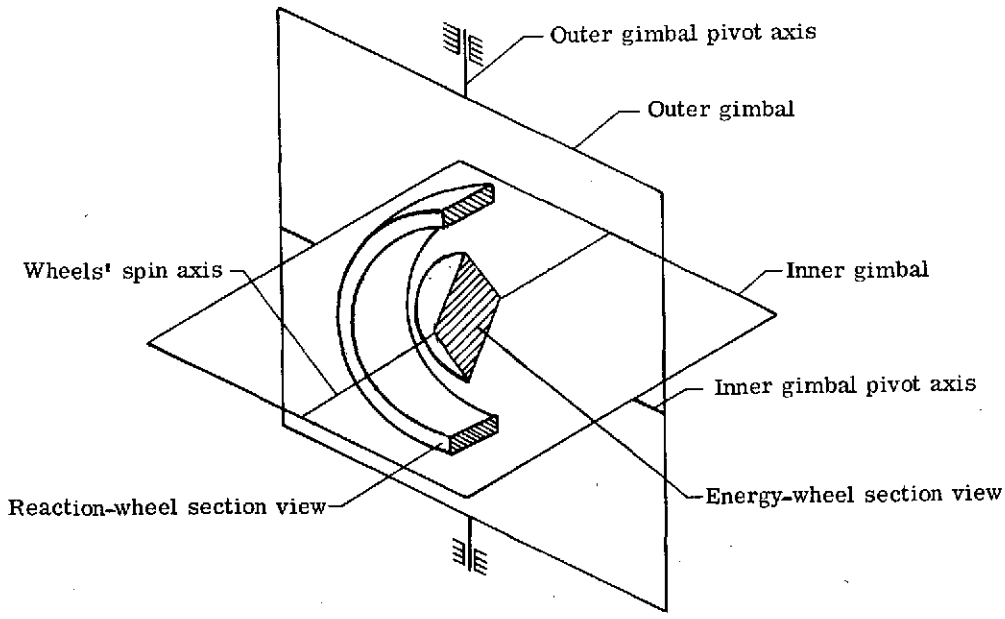

Figure 1. - TAG unit general arrangement.

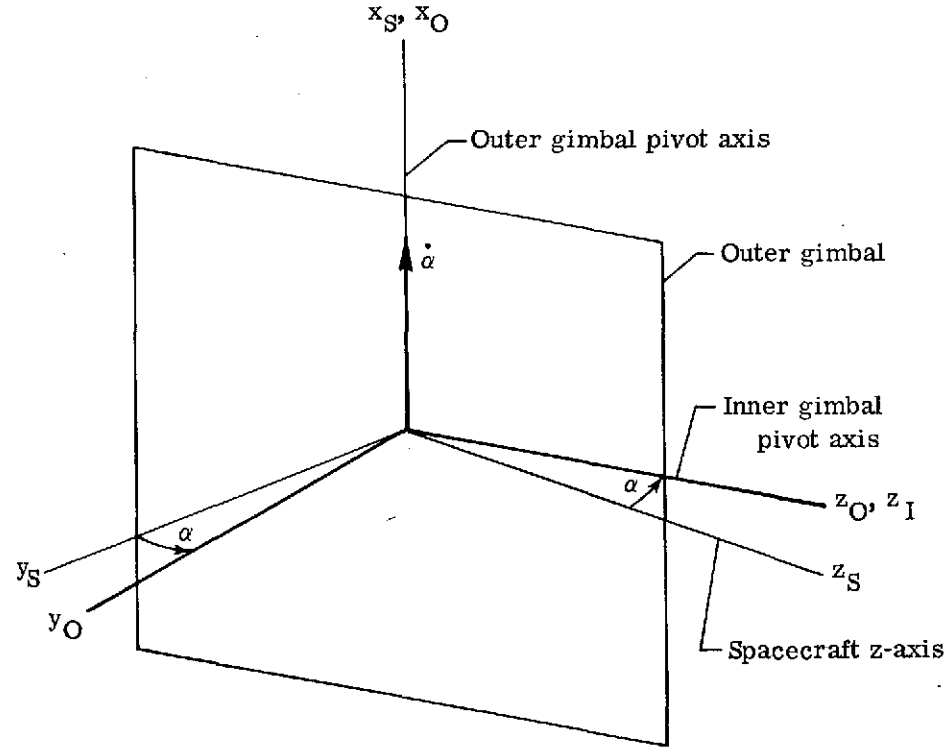

Figure 2. - TAG outer gimbal axis system.

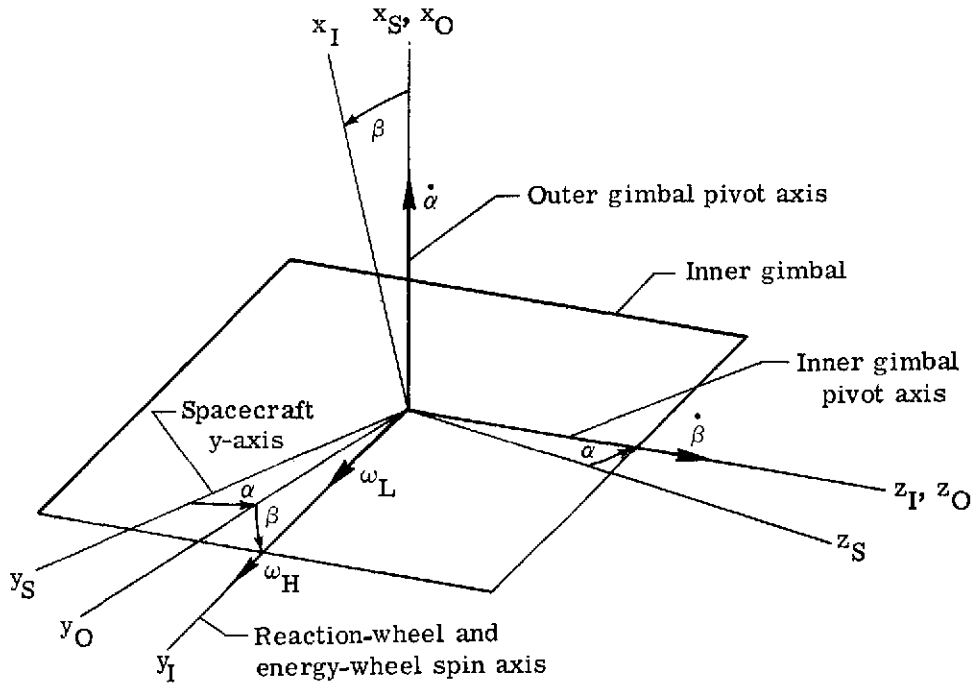

Figure 3. - TAG inner gimbal axis system.

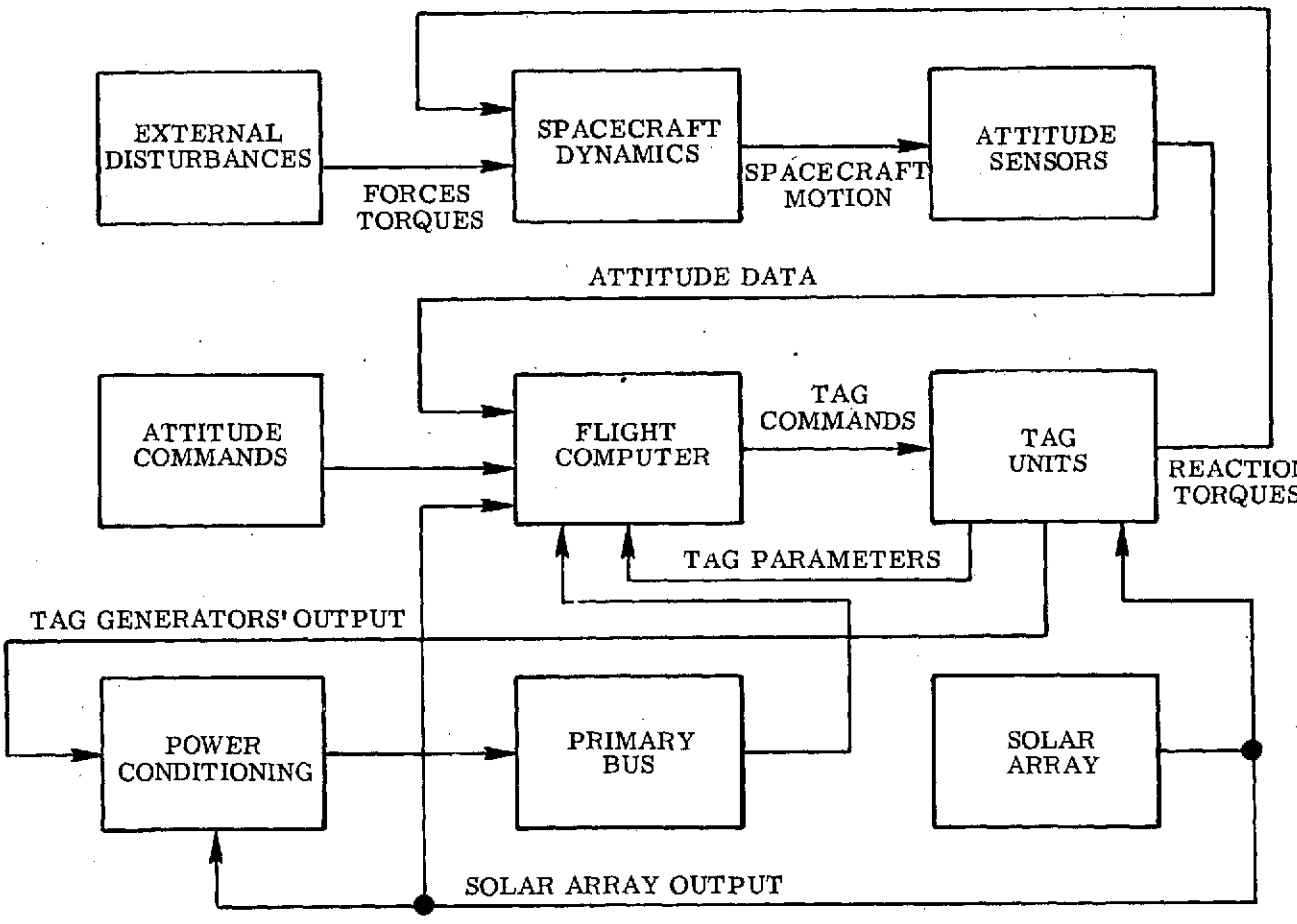

Figure 4. - Spacecraft attitude control and power system block diagram.

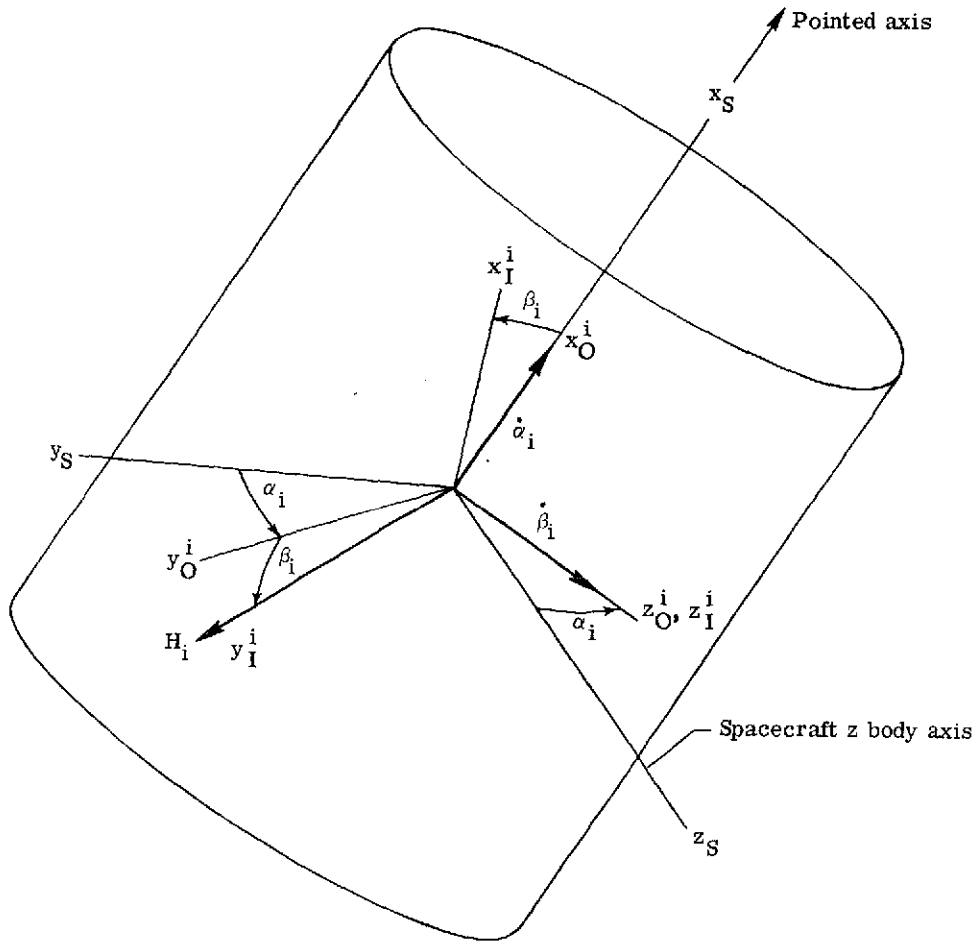

Figure 5. - Spacecraft-TAG axes showing the ith TAG gimbal angles, gimbal rates, and angular momentum.

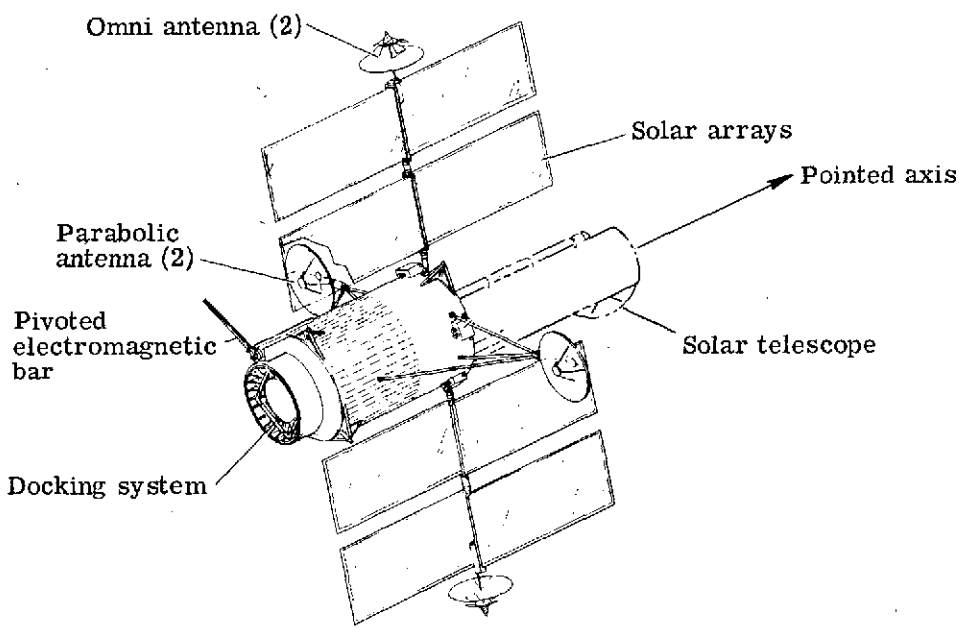

Figure 6. - Example free-flying RAM general arrangement.

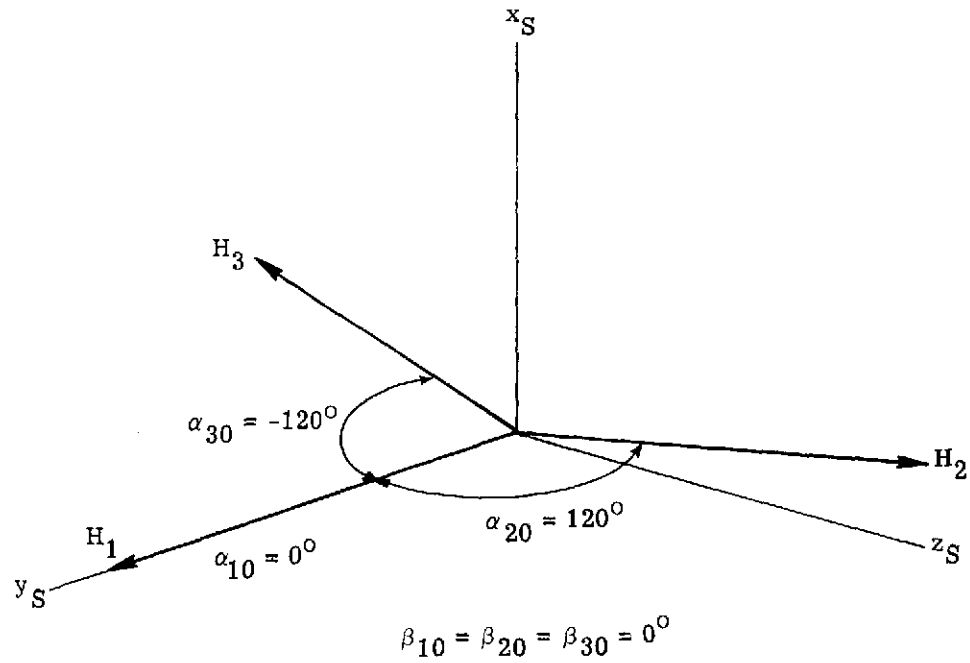

Figure 7. - RAM-TAG reference gimbal orientations.

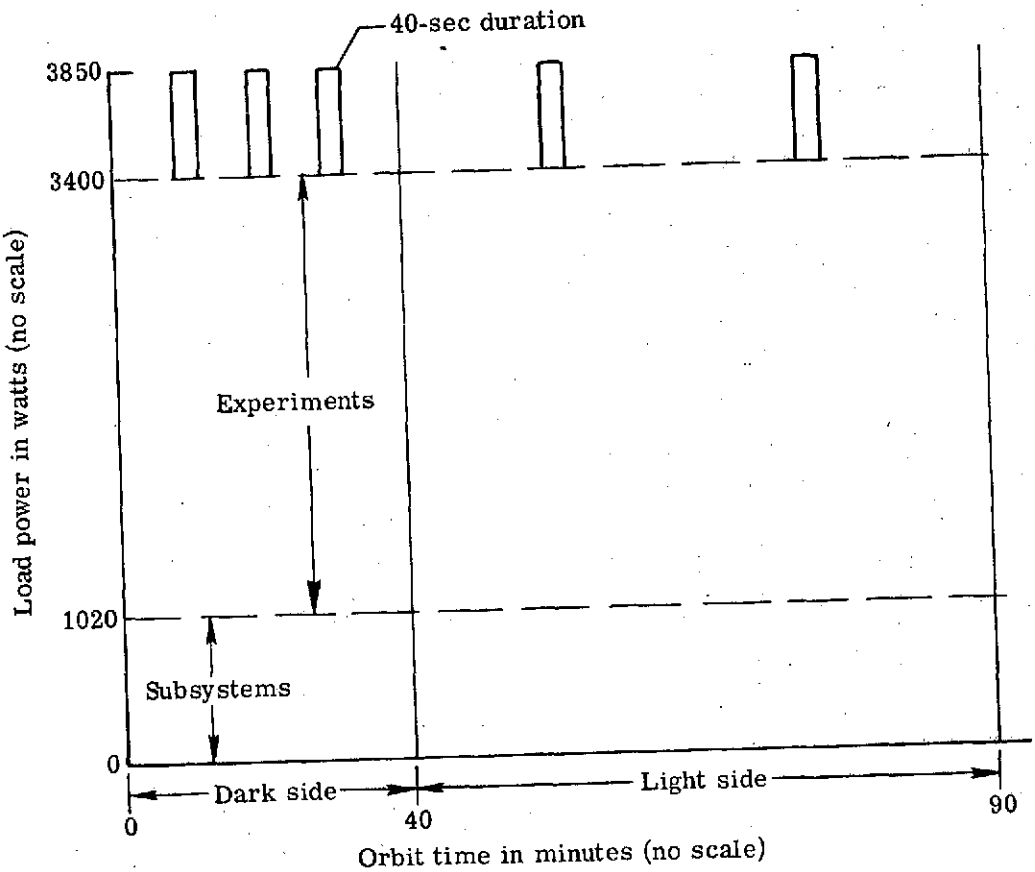

Figure 8. - Example power profile for simultaneous operation of experiments.

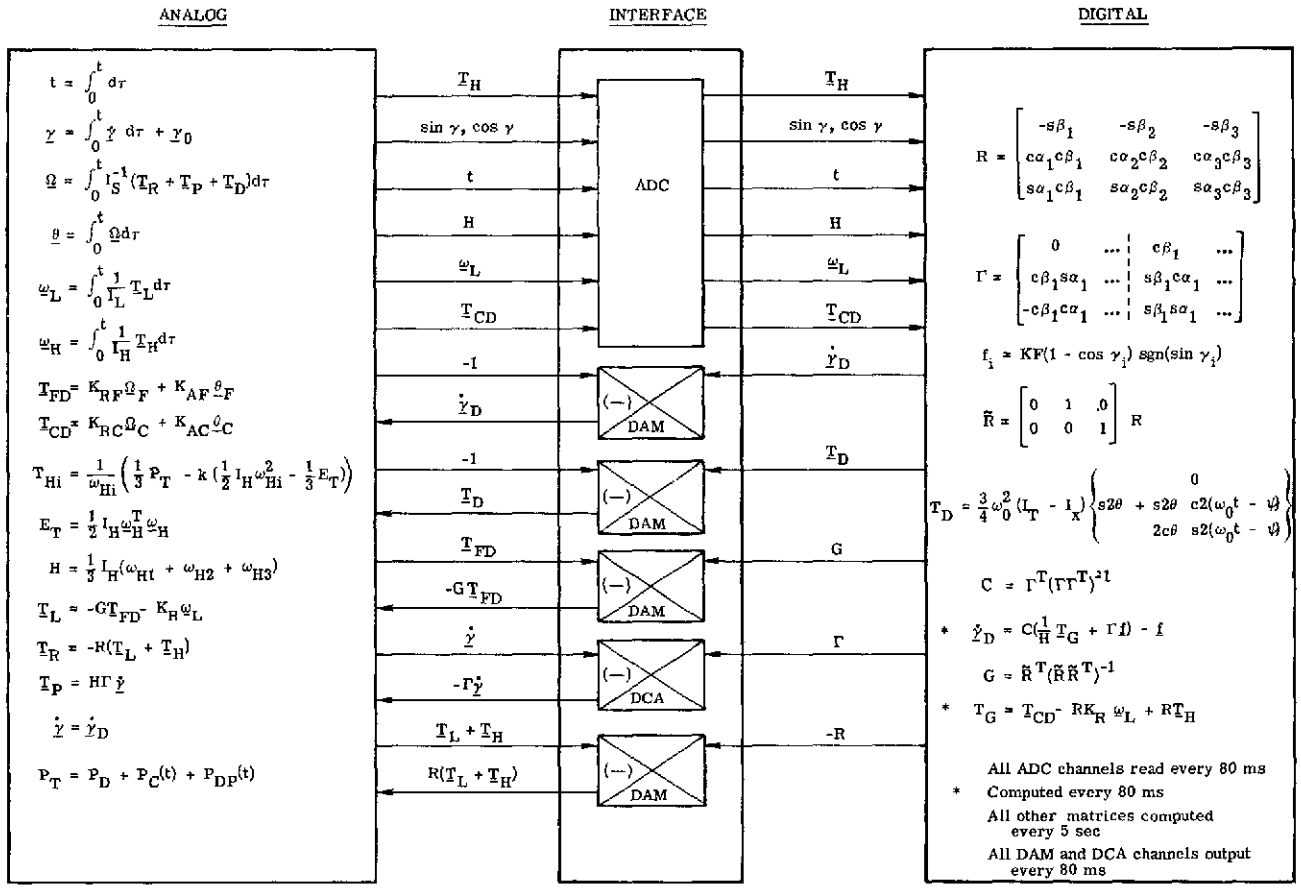

Figure 9. - RAM-TAG system simulation block diagram.

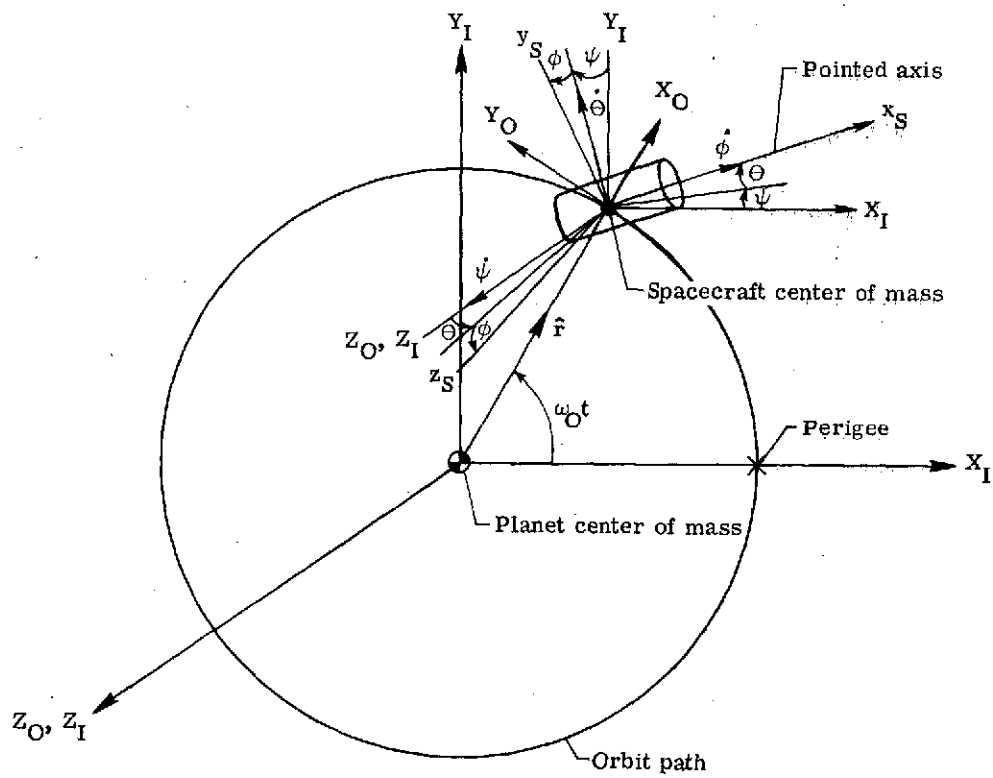

Figure 10. - Orientation of coordinate axes. Order of Euler rotations is ψ, θ, and ϕ.

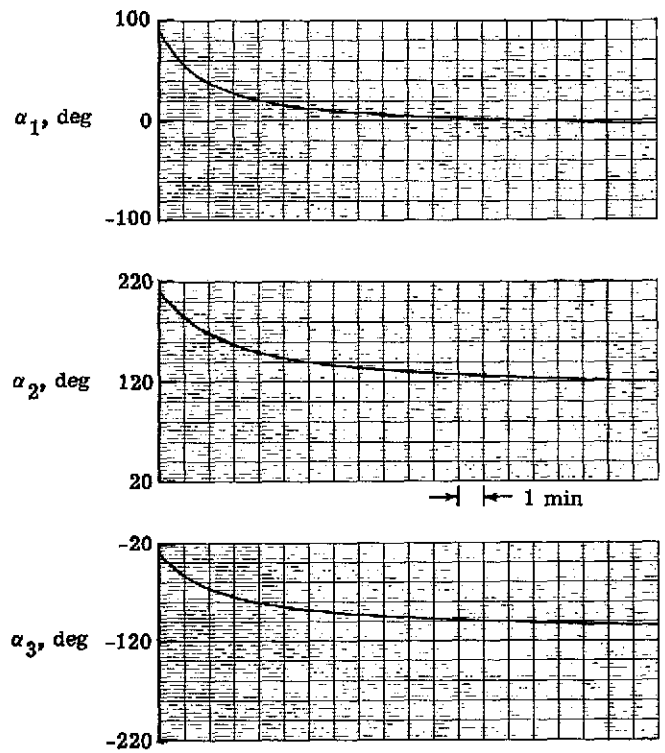

(a) Outer gimbal angle responses.

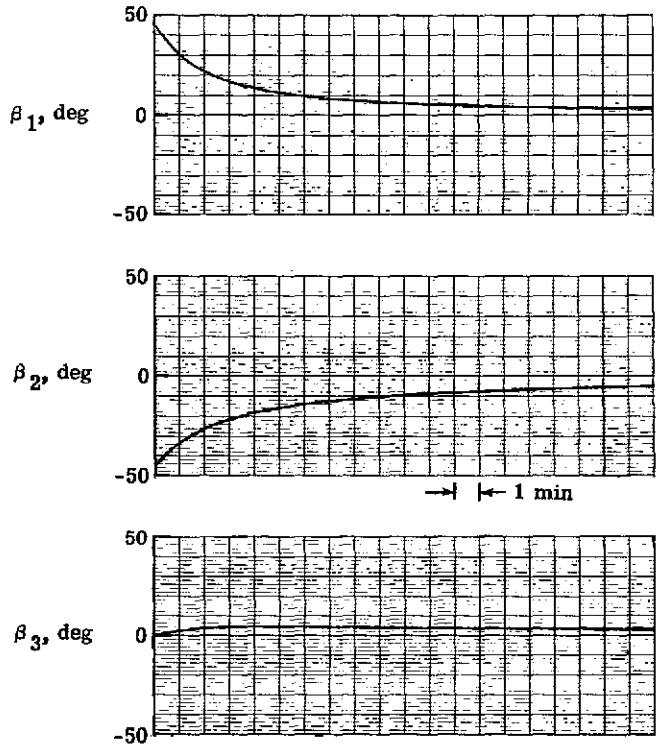

(b) Inner gimbal angle responses.

Figure 11. - Gimbal angle minimization case with $\alpha_1 = 90^o$, $\alpha_2 = 210^o$, $\alpha_3 = -30^o$, $\beta_1 = 45^o$, $\beta_2 = -45^o$, $\beta_3 = 0^o$, $\omega_{Hi} = 25\,000$ rpm, and $\omega_{L1} = 0$ initially, and without gravity-gradient or power-transfer torques.

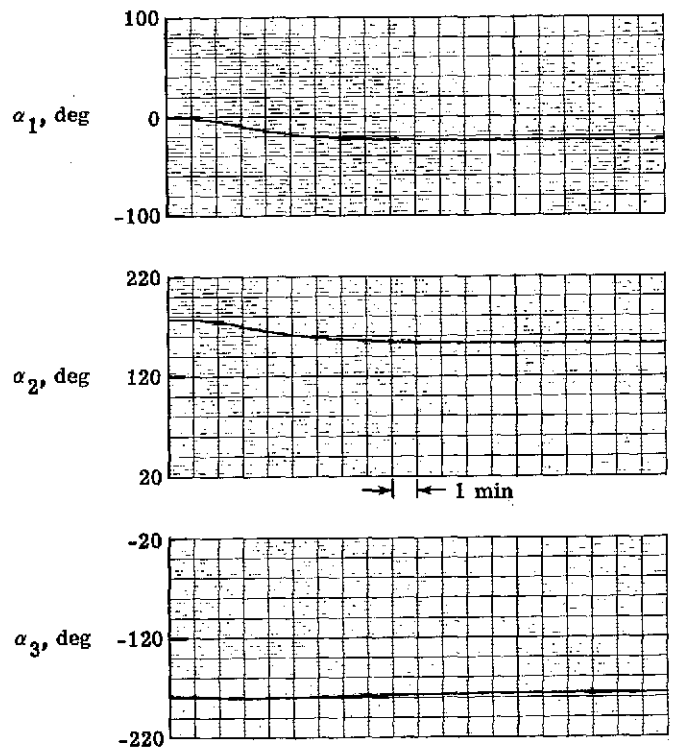

(a) Outer gimbal angles responses.

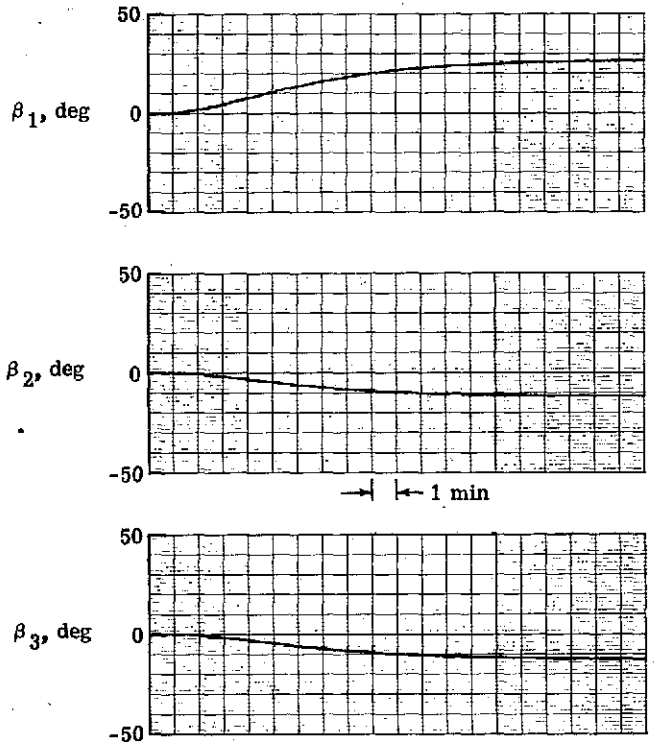

(b) Inner gimbal angle responses.

Figure 12. - Gimbal angle minimization case with $\alpha_1 = 0^o$, $\alpha_2 = 176^o$, $\alpha_3 = -176^o$, $\beta_i = 0^o$, $\omega_{Hi} = 25\,000$ rpm, and $\omega_{Li} = 0$ initially, and without gravity-gradient or power-transfer torques.

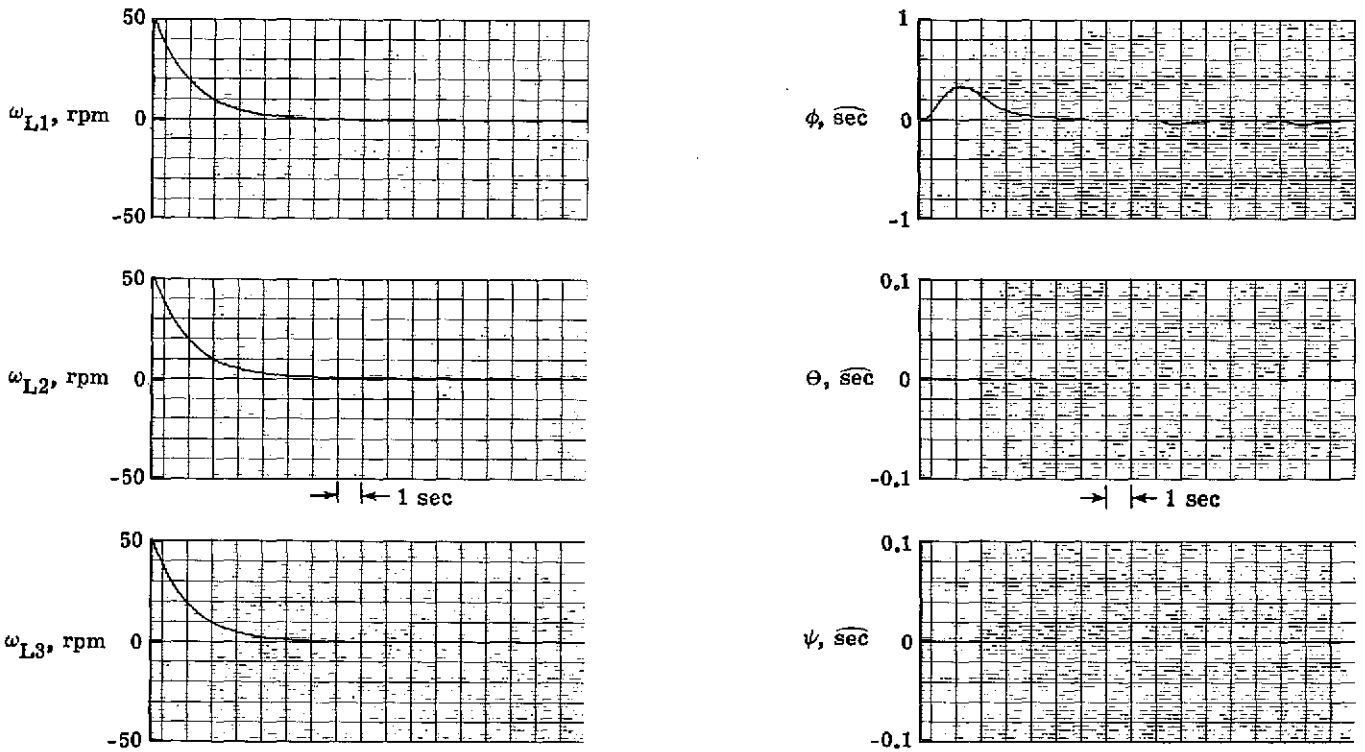

(a) Reaction wheel speeds.

(b) Spacecraft pointing errors.

Figure 13. - Reaction-wheel desaturation case with $\alpha_1 = 0^{\circ}$, $\alpha_2 = 120^{\circ}$, $\alpha_3 = -120^{\circ}$, $\beta_i = 60^{\circ}$, $\omega_{Li} = 50$ rpm, and $\omega_{Hi} = 25\,000$ rpm initially, and without gravity-gradient or power-transfer torques.

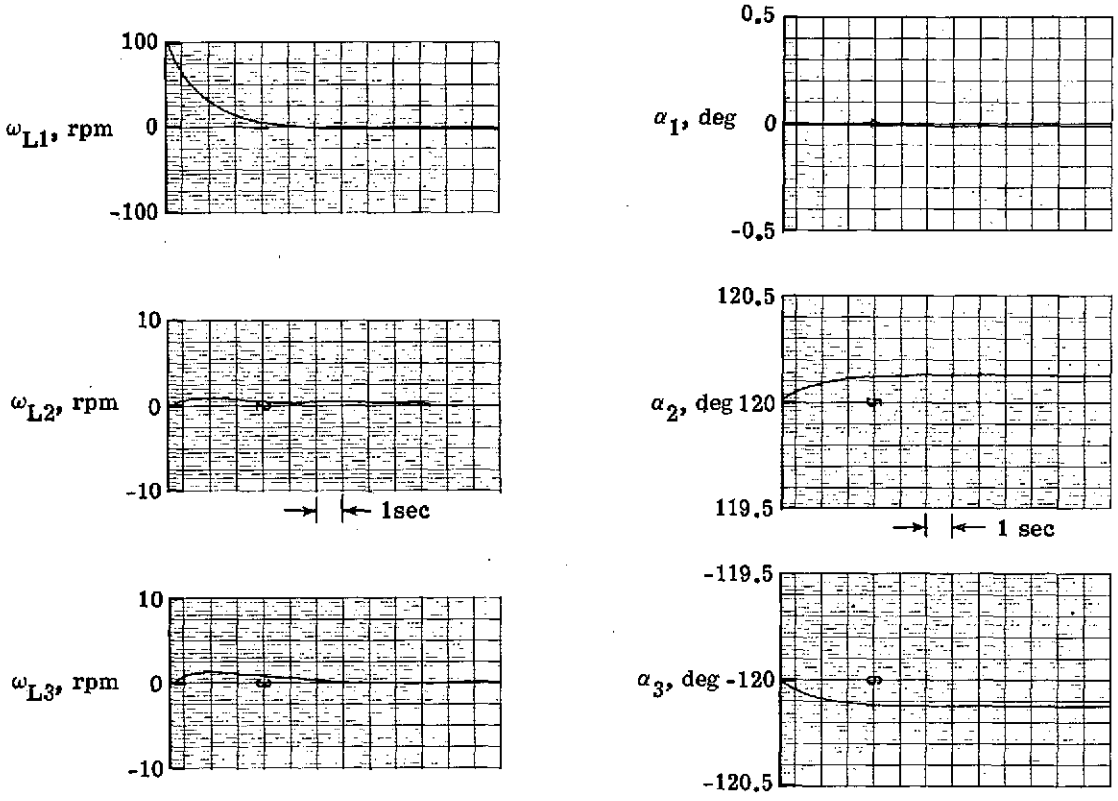

(a) Reaction-wheel speeds.

(b) Outer gimbal angles.

Figure 14. - Reaction-wheel desaturation case with $\omega_{L1} = 100$ rpm, $\omega_{L2} = \omega_{L3} = 0$, $\alpha_1 = 0^o$, $\alpha_2 = 120^o$, $\alpha_3 = -120^o$, $\beta_i = 0^o$, and $\omega_{Hi} = 25\,000$ rpm initially, and without gravity-gradient or power-transfer torques.

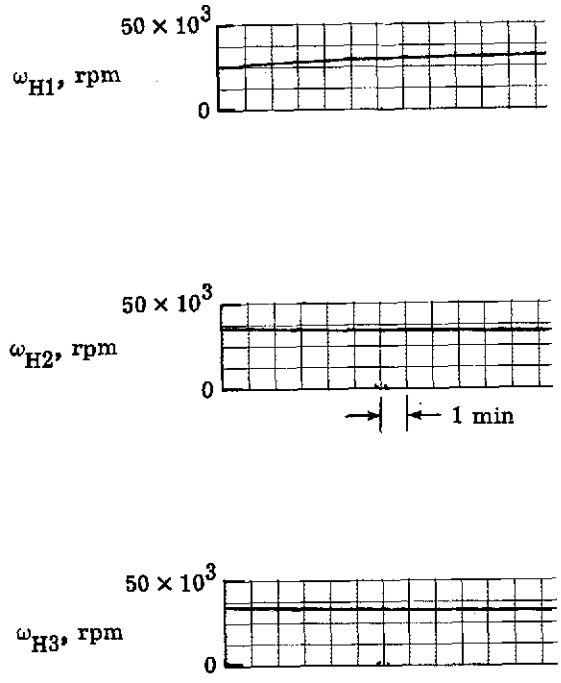

(a) Energy-wheel speeds.

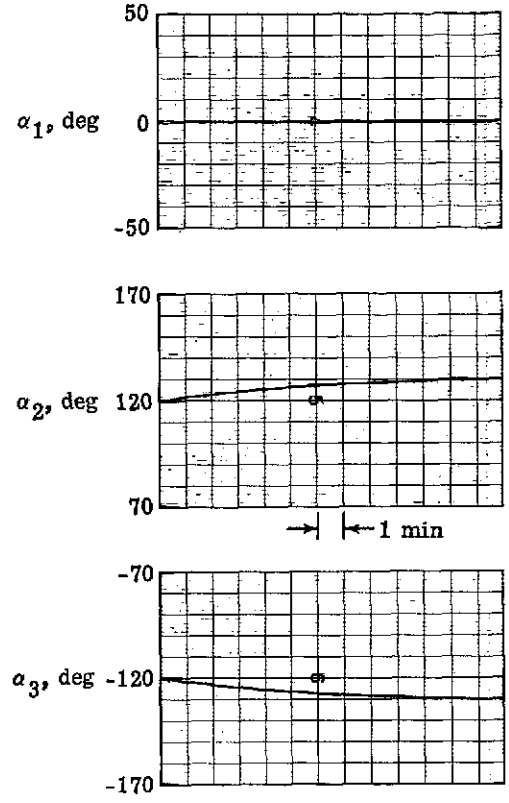

(b) Outer gimbal angles.

Figure 15.- Energy-wheel speed equalization case with ω_{H1} = 25 000 rpm, $\omega_{H2} = \omega_{H3}$ = 35 000 rpm, $\omega_{Li} = 0$, $\alpha_1 = 0^o$, $\alpha_2 = 120^o$, $\alpha_3 = -120^o$, and $\beta_i = 0^o$ initially, and without gravity-gradient or power-transfer torques.

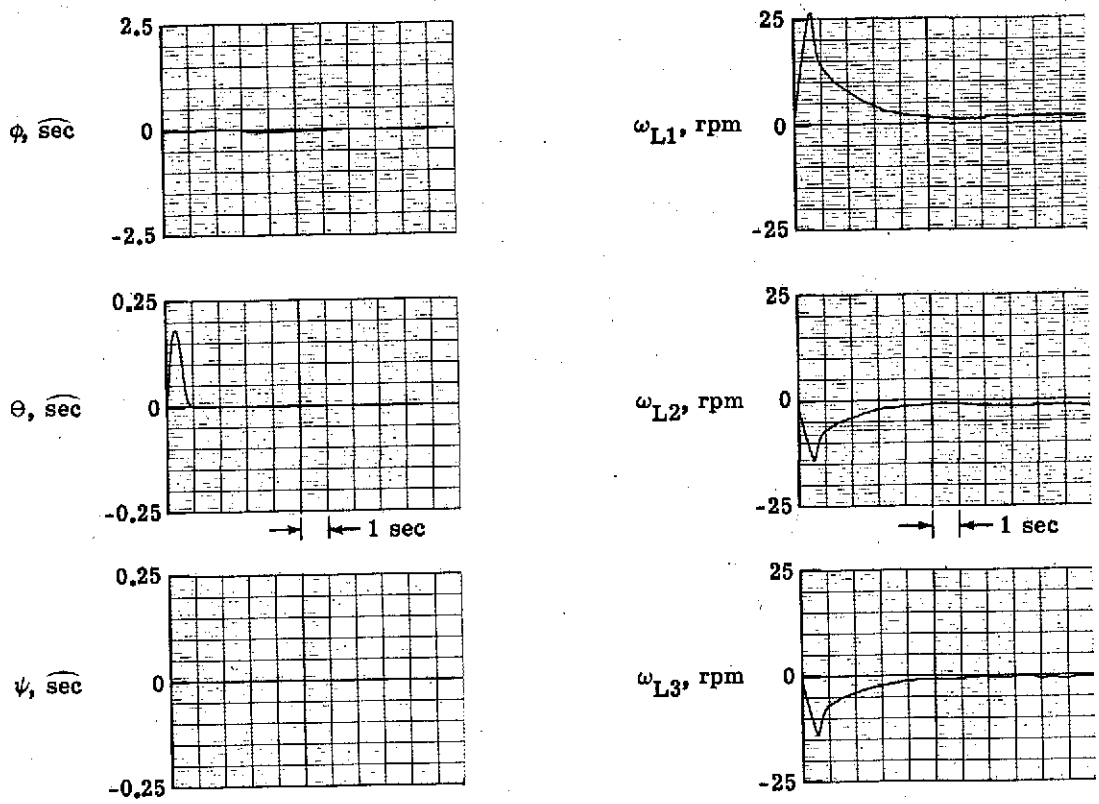

(a) Spacecraft pointing errors.

(b) Reaction-wheel speeds.

Figure 16. - Spacecraft y_S (pitch) axis 2 N-m-sec impulsive disturbance case with $\omega_{Li} = 0$, $\omega_{Hi} = 25\,000$ rpm, $\alpha_1 = 0^o$, $\alpha_2 = 120^o$, $\alpha_3 = -120^o$, and $\beta_1 = 0^o$ initially, and without gravity-gradient or power-transfer torques.

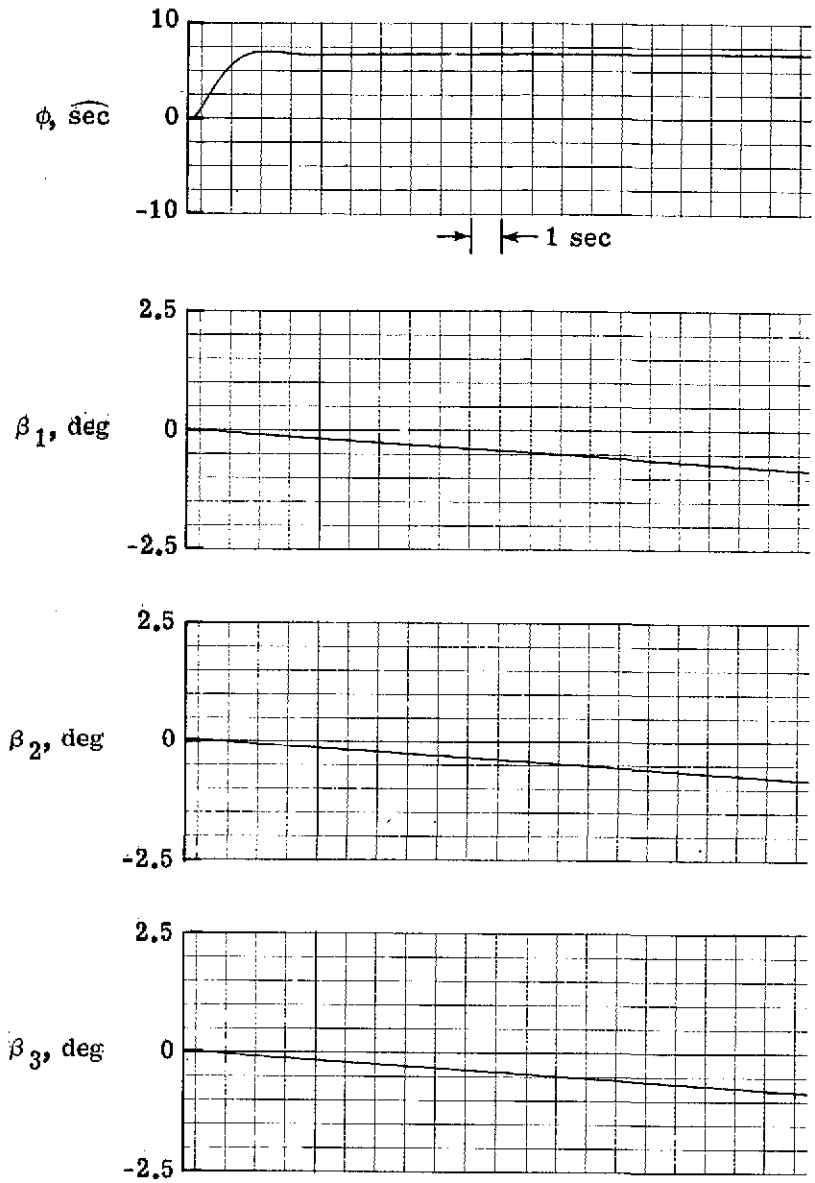

Figure 17. - Spacecraft x_S (roll) axis 2.74 N-m constant disturbance case with $\alpha_1 = 0^o$, $\alpha_2 = 120^o$, $\alpha_3 = -120^o$, $\beta_i = 0^o$, $\omega_{Li} = 0$, and $\omega_{Hi} = 25\,000$ rpm initially, and without gravity-gradient or power-transfer torques.

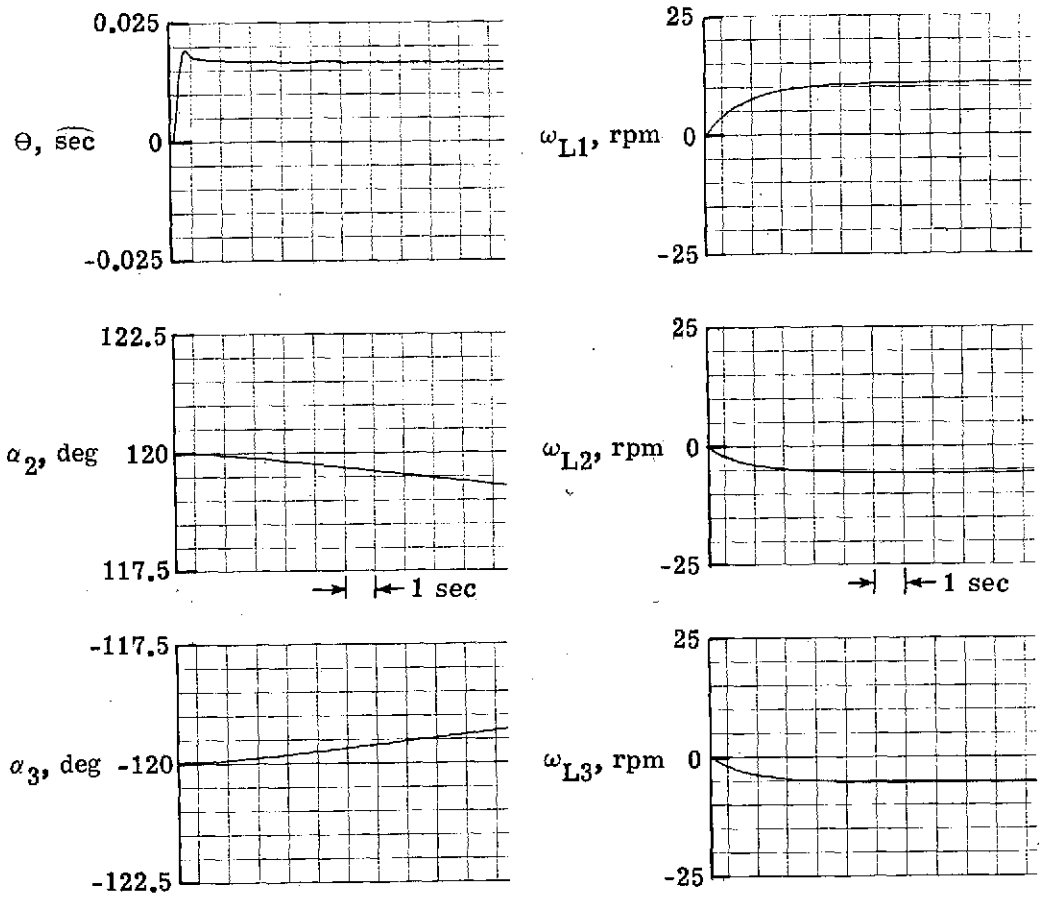

Figure 18. - Spacecraft y_S (pitch) axis 2.74 N-m constant disturbance case with $\alpha_1 = 0^o$, $\alpha_2 = 120^o$, $\alpha_3 = -120^o$, $\beta_i = 0^o$, $\omega_{Hi} = 25\,000$ rpm, and $\omega_{Li} = 0$ initially, and without gravity-gradient or power-transfer torques.

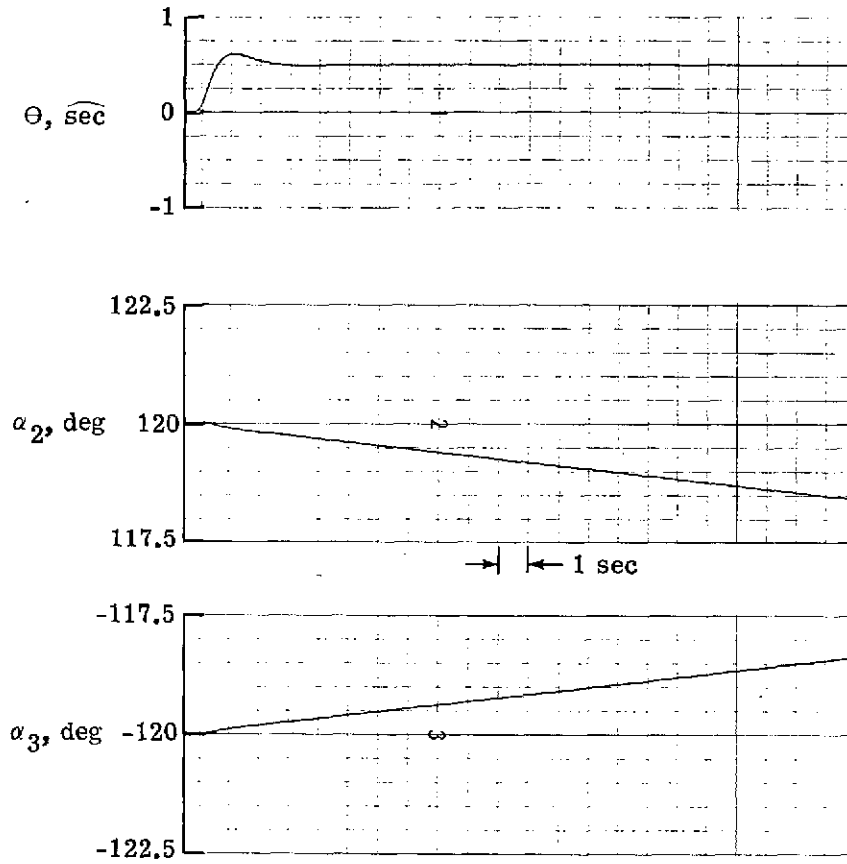

Figure 19. - Spacecraft y_S (pitch) axis 2.74 N-m constant disturbance case without fine pointing control with $\alpha_1 = 0^o$, $\alpha_2 = 120^o$, $\alpha_3 = -120^o$, $\beta_i = 0^o$, $\omega_{Hi} = 25\,000$ rpm, and $\omega_{Li} = 0$ initially, and without gravity-gradient or power-transfer torques.

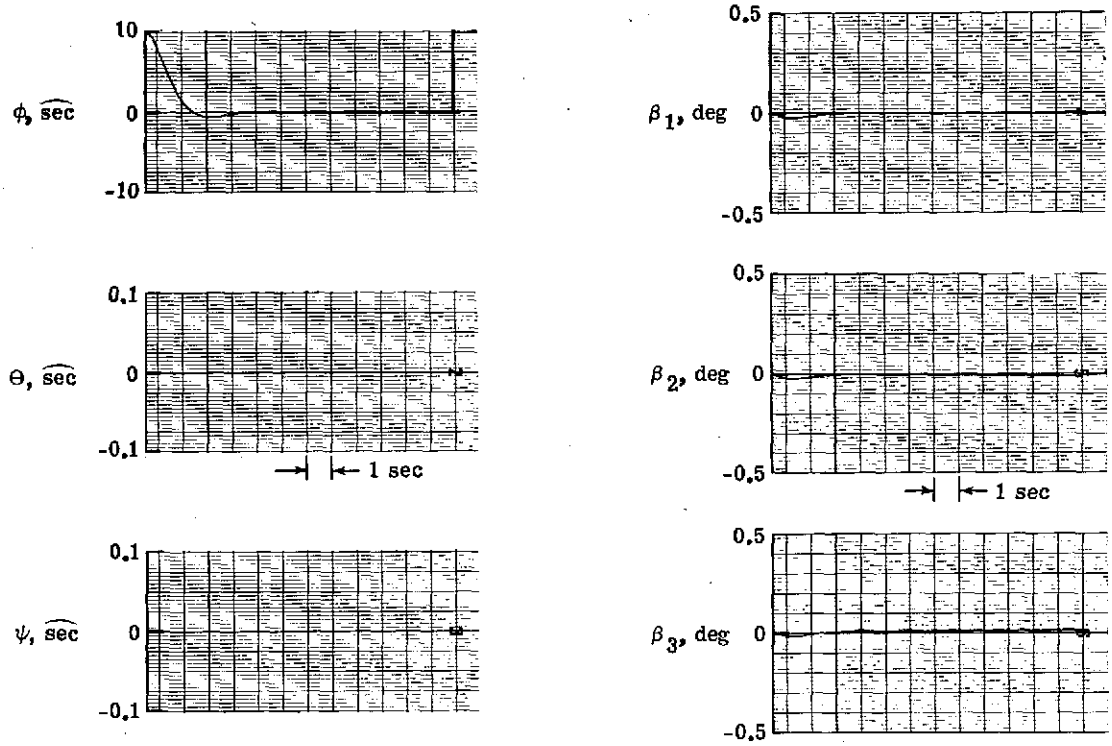

(a) Spacecraft pointing errors.

(b) Inner gimbal angles.

Figure 20. - Spacecraft x_S (roll) axis initial pointing error case with $\alpha_1 = 0^o$, $\alpha_2 = 120^o$, $\alpha_3 = -120^o$, $\beta_i = 0^o$, $\omega_{Hi} = 25\,000$ rpm, $\omega_{Li} = 0$, $\phi = 10$ arc sec, and $\theta = \psi = 0$ initially, and without gravity-gradient or power-transfer torques.

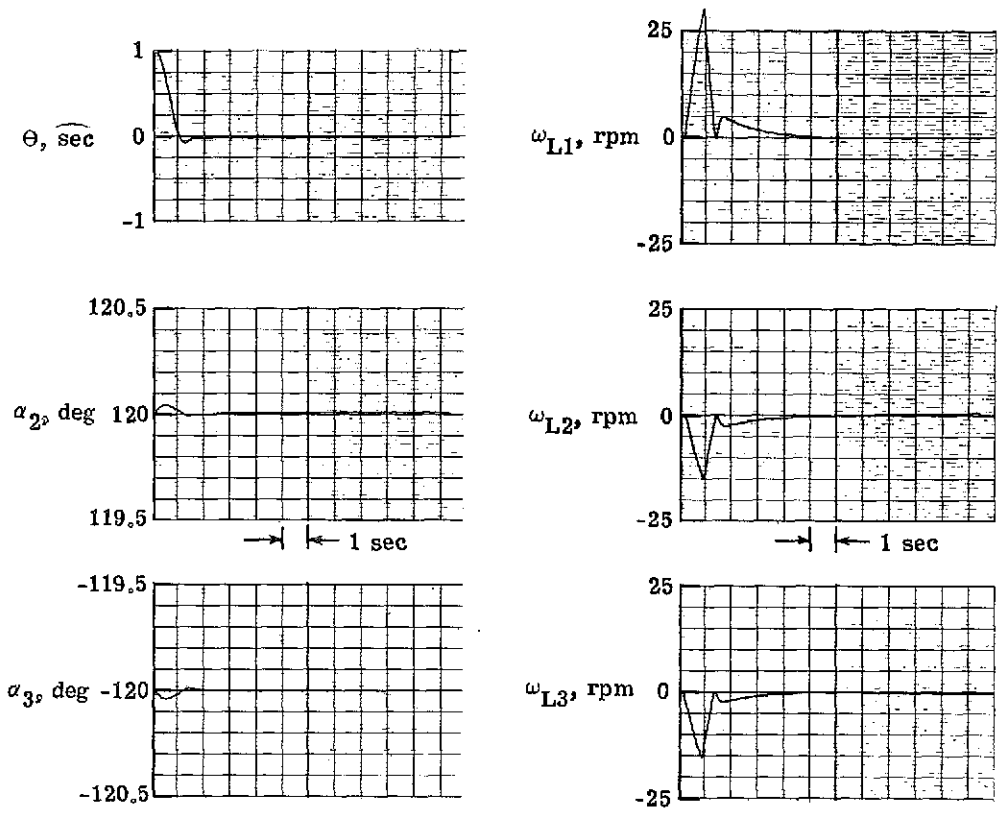

Figure 21. - Spacecraft y_S (pitch) axis initial pointing error case with $\alpha_1 = 0^o$, $\alpha_2 = 120^o$, $\alpha_3 = -120^o$, $\beta_i = 0^o$, $\omega_{Hi} = 25\,000$ rpm, $\omega_{Li} = 0$, $\phi = \psi = 0$, and $\theta = 1$ arc sec initially, and without gravity-gradient or power-transfer torques.

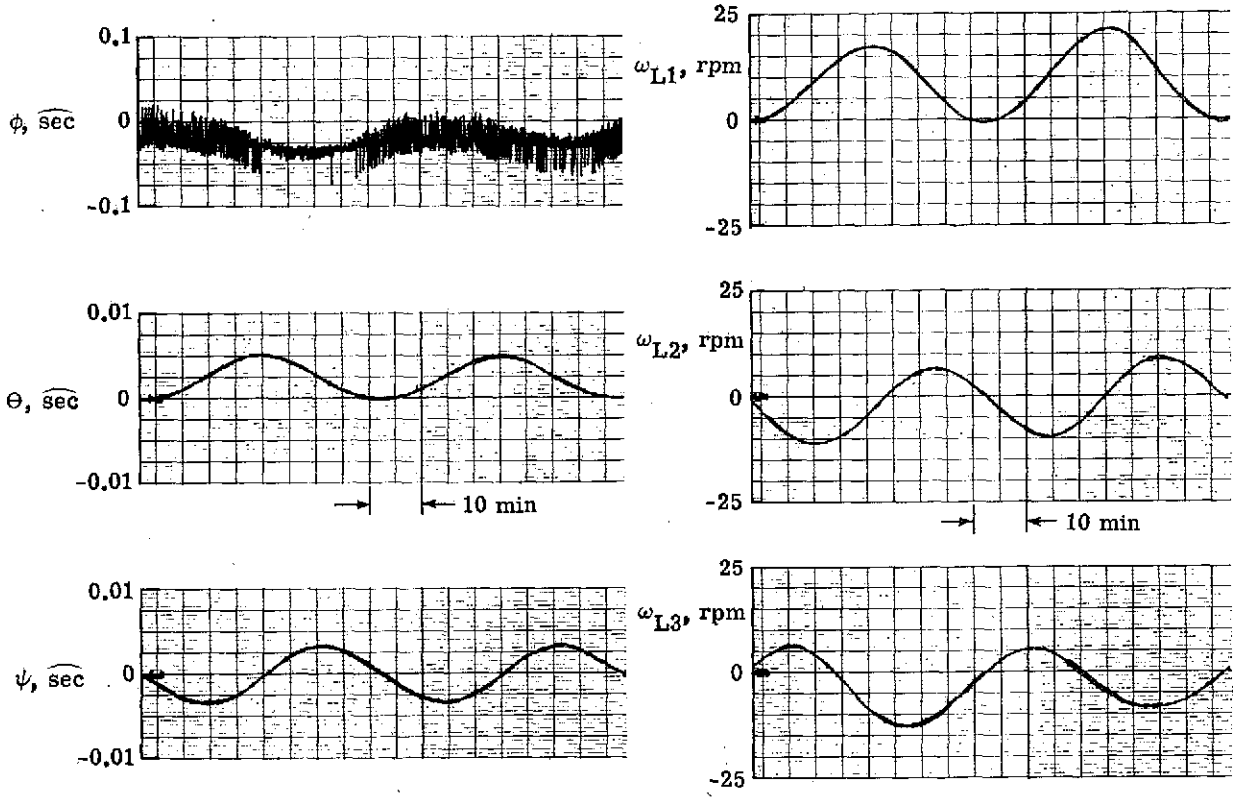

(a) Spacecraft pointing errors and reaction-wheel speeds.

Figure 22. - Spacecraft orbit case with $\phi_O = 0^O$, $\theta_O = 45^O$, $\psi_O = 90^O$, $\alpha_1 = 0^O$, $\alpha_2 = 120^O$, $\alpha_3 = -120^O$, $\beta_i = 0^O$, $\omega_{Li} = 0$, and $\omega_{Hi} = 25\,000$ rpm initially.

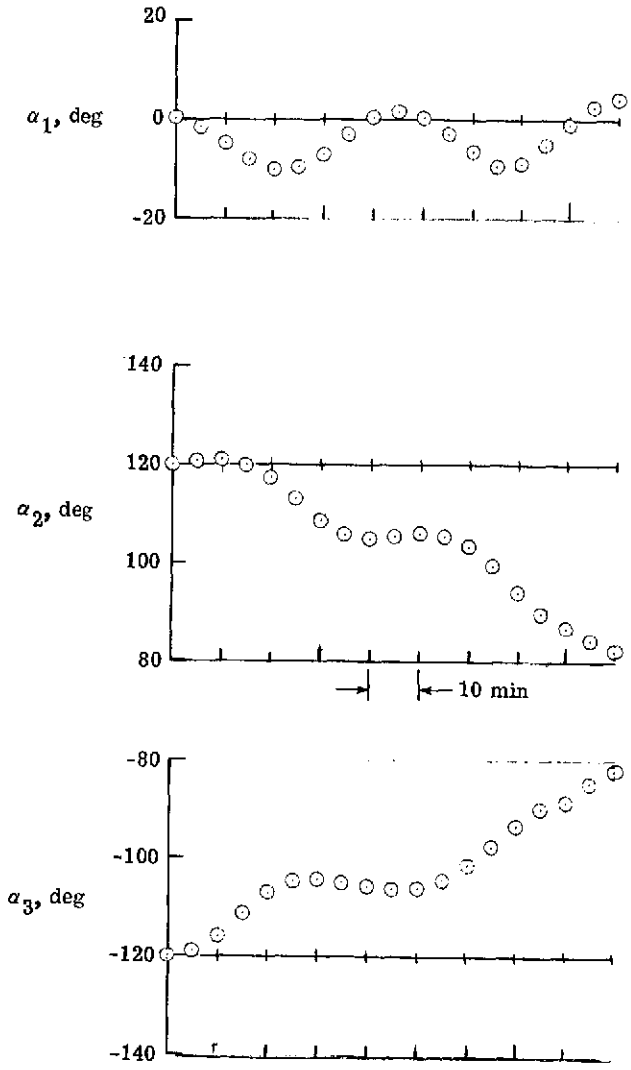

(b) Outer gimbal angles.

Figure 22. - Continued.

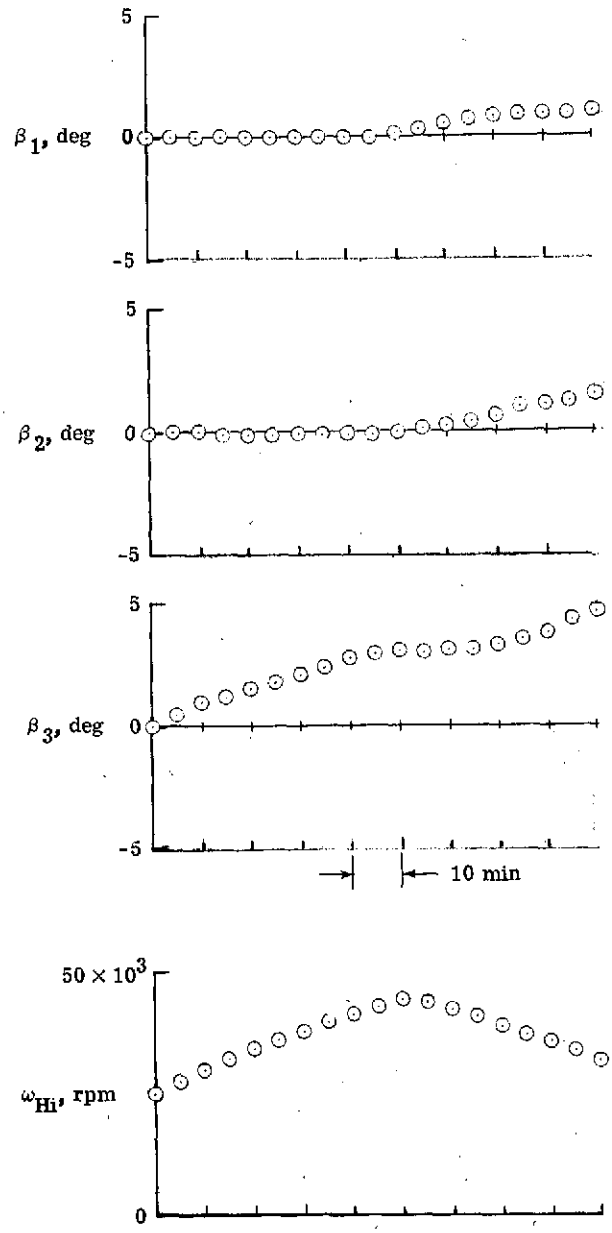

(c) Inner gimbal angles and energy-wheel speeds.

Figure 22. - Concluded.

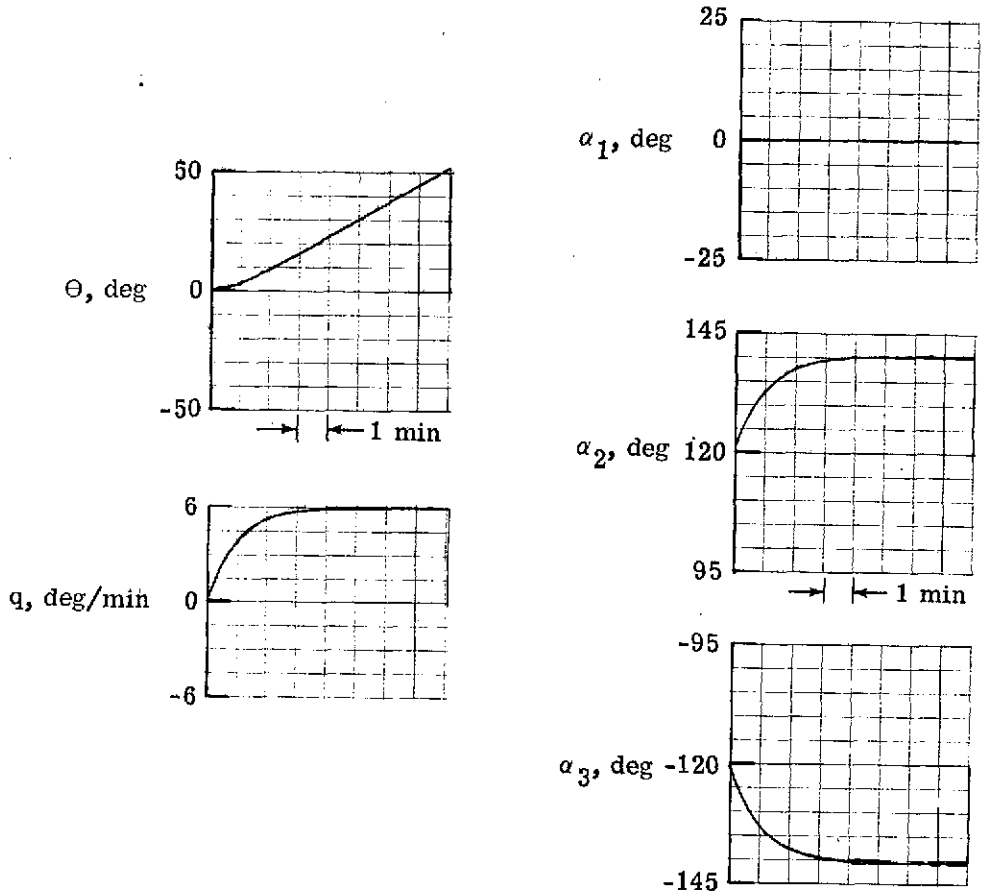

Figure 23.- Spacecraft y_S (pitch) axis reorientation rate acquisition case with $\alpha_1 = 0^o$, $\alpha_2 = 120^o$, $\alpha_3 = -120^o$, $\beta_i = 0^o$, $\omega_{Li} = 0$, and $\omega_{Hi} = 25\,000$ rpm initially, and without gravity-gradient or power-transfer torques.

NASA-Langley, 1974 L-9271